CLAY-BASED PHOTOTHERMAL AGENTS FOR ANTIBACTERIAL APPLICATIONS

by

SENA YÜCE

Submitted to the Graduate School of Engineering and Natural Sciences

in partial fulfillment of the requirements for the degree of Master of Science.

Sabanci University

Spring 2022

CLAY-BASED PHOTOTHERMAL AGENTS FOR ANTIBACTERIAL APPLICATIONS

APPROVED BY:

DATE OF APPROVAL:26/07/2022

ABSTRACT

CLAY-BASED PHOTOTHERMAL AGENTS FOR ANTIBACTERIAL APPLICATIONS

SENA YÜCE

Materials Science and Nano Engineering, M.Sc. Thesis, July 2022

Thesis Supervisor: Asst. Prof. Hayriye ÜNAL

Keywords: halloysite nanotubes, polydopamine, photothermal agents, light-to-heat conversion, antibacterial activity

Light-to-heat conversion nanoparticles with effective photothermal activity play an important role in the design of photothermal materials that are remotely heated by light. In this thesis, novel clay-based photothermal agents and their utilization as a light-activated antibacterial coating for air filters were presented. By coating them with polydopamine (PDA), a photothermal polymer, halloysite nanotubes (HNTs) were turned into nano-heaters that can be remotely activated by near infrared (NIR) light. HNT-PDA nanohybrids were investigated in terms of their light-activated temperature elevations and were demonstrated to heat up proportionally to the amount of PDA coating on HNTs upon exposure to NIR light. The stability and reusability of the

photothermal activity of the HNT-PDA nanohybrids upon multiple NIR irradiation cycles were studied. *Staphylococcus aureus* (*S. aureus*) treated with HNT-PDA nanohybrids were shown to be physically disrupted upon NIR irradiation resulting in 6.3 log reduction in viability in 5 min irradiation. As a demonstration of the potential use of HNT-PDA nanohybrids in antibacterial applications, their utilization as coatings on air filtration membranes for turning them into light-activated antibacterial air filters was studied. A commercial HEPA filter was spray-coated with HNT-PDA nanohybrids resulting in air filters, which can be heated to temperatures sufficient to kill microorganisms when exposed to NIR light. HNT-PDA nanohybrids coated HEPA filters treated with *S. aureus* presented a 3.4 log killing activity after 20 min NIR irradiation. Furthermore, it was observed that the *S. aureus* biofilm established on the filter surface was eradicated via NIR light exposure. The HNT-PDA coating on the air filter was shown not to negatively affect the filtration performance The HNT-PDA coated air filters presented excellent aerosol filtration efficiency in addition to their bioaerosol removal and deactivation performance. The novel clay-based photothermal agents presented in this thesis have a strong potential for utilization as light-activated antibacterial agents in various applications.

ÖZET

ANTİBAKTERİYEL UYGULAMALAR İÇİN KİL BAZLI FOTOTERMAL AJANLAR

SENA YÜCE

Malzeme Bilimi ve Nano Mühendislik, Yüksek Lisans. Tezi, Temmuz 2022

Tez Danışmanı: Doç. Dr. Hayriye ÜNAL

Anahtar Kelimeler: halloysit nanotüpler, polidopamin, fototermal nanohibritler, ışıktan ısıya, antibakteriyel aktivite

Etkili fototermal aktiviteye sahip ışıktan ısıya dönüşüm nanoparçacıkları, ışıkla uzaktan ısıtılan fototermal malzemelerin tasarımında önemli bir rol oynamaktadır. Bu tezde, yeni kil bazlı fototermal ajanlar ve bunların hava filtreleri için ışıkla aktive olan bir antibakteriyel kaplama olarak kullanımları sunulmuştur. Bir fototermal polimer olan polidopamin (PDA) ile kaplanarak, halloysit nanotüpler (HNT'ler), yakın kızılötesi (NIR) ışıkla uzaktan etkinleştirilebilen nano-ısıtıcılara dönüştürüldü. HNT-PDA nanohibritleri, ışıkla aktive olan sıcaklık yükselmeleri açısından araştırıldı ve NIR ışığına maruz kaldıklarında HNT'ler üzerindeki PDA kaplama miktarıyla orantılı olarak ısındıkları gösterildi. HNT-PDA nanohibritlerinin fototermal aktivitesinin çoklu NIR ışınlama döngüleri üzerindeki kararlılığı ve yeniden kullanılabilirliği incelenmiştir. HNT-PDA nanohibritleri ile tedavi edilen *Staphylococcus aureus*'un (*S. aureus*), 5 dk

ışınlamada canlılıkta 6,3 log azalma ile sonuçlanan NIR ışınlaması üzerine fiziksel olarak bozulduğu gösterilmiştir. HNT-PDA nanohibritlerinin antibakteriyel uygulamalardaki potansiyel kullanımının bir göstergesi olarak, bunların hava filtrasyon membranları üzerinde ışıkla aktive olan antibakteriyel hava filtrelerine dönüştürülmesi için kaplama olarak kullanımları incelenmiştir. Ticari bir HEPA filtresi, NIR ışığına maruz kaldığında mikroorganizmaları öldürmek için yeterli sıcaklıklara ısıtılabilen hava filtreleri ile sonuçlanan HNT-PDA nanohibritleri ile spreyle kaplanmıştır. S. aureus ile muamele edilmiş HNT-PDA nanohibritleri kaplı HEPA filtreleri, 20 dk NIR ışımasından sonra 3.4 log öldürme aktivitesi sergiledi. Ayrıca filtre yüzeyinde oluşan S. aureus biyofilminin NIR ışığına maruz bırakılarak yok edildiği gözlemlendi. Hava filtresi üzerindeki HNT-PDA kaplamanın filtrasyon performansını olumsuz etkilemediği gösterildi. Ek olarak, HNT-PDA kaplı hava filtreleri, biyoaerosol giderimi ve deaktivasyon performanslarında mükemmel aerosol filtrasyon verimliliği gösterdi. Bu tezde sunulan yeni kil bazlı fototermal ajanlar, çeşitli uygulamalarda ışıkla aktive olan antibakteriyel ajanlar olarak kullanım için güçlü bir potansiyele sahiptir..

ACKNOWLEDGEMENTS

I would like to thank my advisor, Asst. Prof. Hayriye Ünal, for her academic and personal support during my master's period. I would like to thank her for encouraging and continuously guiding me in my academic career. Allowed me to improve myself in terms of scientific perspective and to expand my horizons toward scientific approaches. I am very grateful to be part of her research group.

I would like to thank Asst. Prof. Dr. Serkan Ünal, who provided me with an internship opportunity at Sabancı University during my undergraduate period. Thanks to him, an interesting and informative experience has guided me in deciding if I would like to evaluate myself academically.

I would like to thank Dr. Cüneyt Erdinç Taş and Dr. Buket Alkan Taş. They have improved me by sharing their excellent academic knowledge and guiding my academic studies. I would like to thank them for their dedication and help during my academic period. I have always felt their support academically and mentally. Knowing that they are always there for consultation is priceless. I am very honored to be in the same group.

I would like to thank my colleagues in Hayriye Ünal's research group, Öykü Demirel, Selin Öykü Gündoğdu, Sarp Kölgesiz, and our honorary member Neslihan Şişman who I cannot separate from our research group, for their contribution and friendship. Thanks to the support they showed not only academically but also personally, I spent a period in which we found solutions to all difficulties in a cheerful way. I will never forget their friendship and successfully completed of every challenge together.

I would like to thank Tuçe Fidan, Efsun Şentürk, Gizem Beliktay, Pelin Duru, Tuna Alp, Yelda Yorulmaz for their friendship and support. Also, I would like to thank Dr. Ekin Berksun, Dr. Semih Pehlivan and Dr. Deniz Köken for their friendship and motivation, answered the questions in my mind and shared ideas. I would also like to thank the SUNUM family and Evren Abi for accompanying us with his tasty tea and good conversation during breaks.

True friends are like a light that illuminates your path. I would like to thank, Yağmur Büyük, Aygün Sarı, and Deniz Selçuk for always being there for me and supporting me.

I would like to thank my dear family, especially my mother and father, who supported me financially and morally and believed in me in my master's adventure.

I am thankful to TUBITAK for the scholarship and research funding. (Project no: 113O872 Project no: 216M012)

To my dear family and princess cat Diana...

TABLE OF CONTENT

LIST OF FIGURES

LIST OF TABLES

LIST OF ABBREVIATIONS

HNT	:Halloysite Nanotubes
PDA	:Polydopamine
WPU	:Waterborne Polyurethane
PPy	:Polypyrrole
PAN	:Polyaniline
PEG	:Polyethylene Glycol
Au	:Gold
Pd	:Palladium
CNT	:Carbon Nanotube
Ag	:Silver
PTT	:Photothermal Therapy
PDT	:Photodynamic Therapy
NIR	:Near-Infrared Rage
HEPA	:High Efficiency Particulate Air
FT-IR	:Fourier Transform Infrared
TGA	:Thermogravimetric Analysis
DLS	:Dynamic Light Scattering
SEM	:Scanning Electron Microscope
TEM	:Transmission Electron Microscopy
LSPR	:Localized Surface Plasmon Resonance

“It’s all a question of imagination.
Our responsibility begins with the power
to imagine.”

Haruki Murakami

CHAPTER 1. INTRODUCTION

1.1 Thesis Overview

The photothermal effect is a significant concept that involves converting light energy to thermal energy utilizing photothermal conversion materials. The temperature elevations in photothermal materials upon exposure to light has provided vital solutions in many different application areas such as cancer therapy[1], self-healing[2], solar steam generation[3], and killing bacteria[4]. The light-activated heating of photothermal materials is utilized to disrupt tumors, to kill bacteria via hyperthermia, to evaporate water or to obtain temperature-responsive shape memory materials.

In the first part of this thesis, the design and preparation of a novel clay-based photothermal agent, that can be utilized in various different applications as light-activated nano-heaters was studied. The light-activated heating properties and how these can be useful for remote killing of bacteria were investigated.

In the second part of this thesis, utilization of the clay-based photothermal agents as coatings on commercial air filter membranes was demonstrated. Resulting clay-based photothermal agent coated air filters were demonstrated to be effective in bioaerosol removal and light-activated killing of captured microorganisms.

1.2 Photothermal Effect

The major mechanism of photothermal conversion is that the absorbed light is converted to heat energy. Photothermal materials with strong light absorption can exhibit higher local temperature elevations by irradiation[5]. The light absorption spectrum of a material is related to some specific properties. For example, free electrons on the surface of metallic nanoparticles are excited by light absorption at specific wavelengths, known as localized surface plasmon resonance (LSPR), and show higher photothermal properties as a result of oscillation at the same frequency[6 7].

When light with an energy equal to or greater than the bandgap between the conduction band and the valence band is applied to a semiconductor, it absorbs photons. Afterward, this energy is distributed to the crystal lattice, resulting in thermal energy and a photothermal effect[8].

Another way of light absorption based photothermal effect is lattice vibrations in carbon and polymer-based materials. The incoming light energy can easily excite electrons in the lower energy π orbital and rise to a higher energy orbital by light absorption of the exciting electrons[9]. This causes vibration in the atomic lattices and an increase in temperature is observed[10].

Photothermal materials are roughly separated into two groups. These are organic and inorganic photothermal materials.

1.2.1 Photothermal Materials

1.2.1.1 Organic Photothermal Materials

Organic materials with photothermal effects can be categorized as polymers and dyes. Thanks to their high degree of biocompatibility and low cytotoxicity, organic photothermal materials have achieved high success, especially in biomedical applications [11].

Organic dyes with strong NIR absorption and partial conversion of optical energy into heat are preferred as photothermal agents[12]. There are dye derivatives that are frequently used in fluorescent imaging and photothermal therapy[13]. Compared with polymers or metal nanoparticles, the low stability of dyes is a major disadvantage in cancer treatment [14]. The most widely used cyanine derivatives (IR780, IR825, and IR820) have been encapsulated in various nanocarriers such as micelles, liposomes, polymers, and proteins[11,15]. Cyanine derivatives that have been approved by the USA Food and Drug Administration (FDA) for clinical use in imaging and cancer treatments continue to be investigated in vivo and in vitro[16].

Besides dyes, conjugated polymers including polypyrrole (PPy), polyaniline (PAN), polydopamine (PDA), etc. present photothermal effect[5]. Upon excitation, the π-orbital electrons rise to the high energy orbital resulting in the conversion of light energy into thermal energy and heat production[17].

Unlike NIR dyes, conjugated polymers are opted for cancer treatment and for use as drug carriers because of their high stability and non-toxicity[11,18]. PAN nanoparticles are the first photothermal conjugated polymer used for cancer ablation[1]. However, PAN, which is affected by pH due to the neutralization of protons, loses its photothermal effect over time. To prevent this situation, it was synthesized with stabilizer agents to keep it stable[5].

Another conjugated polymer PPy is used in biomedical and bioelectronic applications and has received great attention for its high conductivity, remarkable stability, and biocompatibility[19]. The cells were incubated with PPy nanoparticles and then exposed to 808 nm NIR light to determine the role of PPy in cell death through heat conversion, and it was reported that around 60-85 % of the cells have died[20].

PDA is produced by the polymerization of dopamine molecules inspired by the sticky form of mussels[21]. It is used as a coating material on surfaces due to its high adhesion property and also as a photothermal agent in coatings due to its high NIR absorption properties. PDA has helped to impart the desired properties to metal and carbon-based materials by coating their surfaces [22]. For example, PDA coatings modified the water solubility of CNTs[23]. Besides, the photothermal effect of PDA has opened up new opportunities in biomedical fields[22].

1.2.1.2 Inorganic Photothermal Materials

Examples of inorganic photothermal materials are metal nanostructures[24–26] ceramic nanoparticles[27–29] and quantum dots[30–32]. Metal nanostructures, which are frequently used today, have excellent abilities in converting light energy into thermal energy, thanks to their LSPR feature[5]. LSPR depends on many properties of metals such as morphology, size, composition, and dielectric constant. The metals with the greatest photothermal properties are known as gold and silver[33]. Gold is found in different sizes and shapes such as nanorods[34–37], nanocages[38–41], and nanoshells[42–46]. Gold nanoparticles with an absorption spectrum between 400 and 600 have shifts in the absorption spectrum of different shapes and sizes[47]. When aggregates form in nanoparticles, the surface plasmon absorption maximum is redshifted to the NIR region[48]. The absorption spectra of gold nanorods and nanoshells are compared, and a significant shift is observed in the LSPR wavelength of the nanorods depending on the aspect ratio[49]. In addition, when the gold surfaces were replaced with smart polymers with stronger bonding, shifts were observed in the absorption peaks. Thus, changes are made in the LSPR spectra according to the NIR region to be used[50]. Gold nanoparticles are frequently used in the field of photothermal therapy because of their biocompatibility, small diameters, direct application to the tumor surface, and the

ability to bind to desired molecules via bioconjugation chemistry[51]. By irradiating with a NIR light source (650-900 nm), a local temperature increase is observed in a certain region [52]. Thus, minimal light absorption in the skin and tissues enables selective tumor tissue hyperthermia without damaging the healthy tissue[53–55]. Gold nanoparticles are also used in cancer imaging due to their unique light-scattering property[56]. With their small sizes the antibody-conjugated nanorods bind specifically to cancer cells and their binding to other healthy cells is minimal. For this reason, it shows high efficiency in the field of cancer imaging.[57,58]

In addition to gold, silver nanoparticles and silver nanostructures are also used in antibacterial applications[59–61], medical imaging[62] and wound healing[63]. Silver, which has the highest electrical and thermal conductivity among metals, is used in photothermal and thermolytic laser applications in cancer treatment with its high NIR region scattering and absorption when looking at the LSPR spectrum.[64,65]The light-to-heat conversion properties of silver has provided an opportunity for wound healing and tissue ablation therapies. In medical area, silver nanoparticles are used in surface coatings, especially in the field of dentistry, coating titanium implants with silver nanoparticles provides a long-term antibacterial effect[66].

1.2.1.3 Carbon-Based Photothermal Materials

Carbon-based photothermal materials are include graphene, graphene oxide, carbon black, graphite, carbon nanotubes (CNTs), and carbon composites[67]. The photothermal mechanism is as follows. When the photon energy of the applied light is higher than the bandgap of the carbon-based material, the photon energy is absorbed. This causes the excitation of electrons and electron-phonon coupling[9]. Diamond, graphene, and CNTs have perfect sp^3 and sp^2 lattice structures and are produced by heat lattice vibration. In amorphous carbon, the disorder affects the phonon scattering and the thermal conductivity[68]. Apart from that, other features it has are high physical and chemical stability, thermal conductivity, and high mechanical strength. It is also cheaper and more abundant than metal materials[67]. In particular, graphene/graphite and CNTs are frequently used in the field of solar steam generation[69–74] apart from metals[75]. They have produced rapid water evaporation as a result of exposure to light due to their

strong absorption band and light-to-heat conversion characteristics [76–78]. In addition, high-efficiency solar absorbers can be produced with the carbonization process applied to natural woods [13,79], and mushrooms[80–82]. The high light absorption property of CNTs is used also in biological applications which are bioimaging, drug delivery, cancer treatment, etc. [83]. With the high absorption, they convert the light energy from near-infrared (650-900 nm) irradiation into heat energy and disrupt the targeted tumor area[84]. In the field of drug delivery, functionalization of the high surface area of CNTs with anti-cancer drugs or bio/chemical species reduces their toxicological value and can deliver drugs by molecular cargo binding [85,86]

1.3 Application of Photothermal Agents as Surface Coatings for Various Applications

Organic, inorganic, and carbon-based materials with photothermal properties have different application areas as mentioned above. In the literature, many examples where photothermal agents are applied in the form of surface coatings were found.

Bone implants and catheters are used for therapeutic purposes in medical applications. After orthopedic surgery, infections on the implant surface penetrates the surrounding tissues, therefore complicating the treatment process and posing a serious [87,88]. As a way of eliminating biofilm infections, the implant surfaces are coated with photothermal agents (polydopamine, polyaniline, gold, etc.) which have biocompatible, non-toxic light-activated antimicrobial properties[89–91]. Thus, the effect of light activated temperature increase on biofilm formation can efficiently prevent biofilm infections and killed the bacteria on implant surfaces[92,93].

Another area of use for surface coating with suitable photothermal agents is to improve the performance of solar collectors via the selective light absorption properties, broad-spectrum absorption, and high photothermal conversion efficiency of photothermal agents[2]. Coating of solar collector film surfaces with copper and carbon-based photothermal agents and coating of the stainless steel mesh-based interface with polypyrrole (PPy), have been shown the performance of solar collectors [94–96].

In a research study to examine long-lasting photothermal coatings, gold nanostars and silver nanoparticles with high NIR absorbance were optimized with biocompatible PVA (polyvinyl alcohol) films, and biocompatible films were tested with viability assay to measure the antibacterial effect on the surface.[61] These research studies show that the coating of any surface with the contribution of photothermal materials with light-heat conversion has created a successful opportunity to obtain an antibacterial surface.[4,97]

1.4 Thesis Structure

This thesis consists of three chapters. Chapter 1 includes a general introduction. Chapter 2 includes a published article ("Yuce, S.; Demirel, O.; Alkan Tas, B.; Sungur, P.; Unal, H. "Halloysite Nanotube/Polydopamine Nanohybrids as Clay-Based Photothermal Agents for Antibacterial Applications". ACS Appl. Nano Mater. 2021, 4 (12), 13432–13439. https://doi.org/10.1021/acsanm.1c02936".) Chapter 3 includes an article that is prepared for submission.

CHAPTER 2. HALLOYSITE NANOTUBE/POLYDOPAMINE NANOHYBRIDS AS CLAY-BASED PHOTOTHERMAL AGENTS

2.1 Abstract

Nanoparticles with light-to-heat conversion properties play vital roles in the design of photothermal materials that can be remotely heated via light activation. Halloysite nanotubes (HNTs), versatile natural clay nanoparticles, were converted into efficient photothermal agents by functionalizing them with polydopamine, a polymer with light-to-heat conversion properties. By varying the polydopamine functionalization reaction conditions such as dopamine concentration, reaction time and the nature of the HNTs, HNT-polydopamine (HNT-PDA) nanohybrids comprising of different amounts of polydopamine were obtained. HNT-PDA nanohybrids presented significant temperature elevations when irradiated with 808 nm laser light reaching 250 °C in 2 min and were demonstrated to be effective photothermal agents, whose light-to-heat conversion properties and the degree of light-activated temperature elevations can be easily tuned by controlling the amount of the polydopamine content through reaction conditions. The photothermal effect of HNT-PDA nanohybrids were demonstrated to be stable over multiple laser light-activation cycles allowing their reusability. In addition to infrared laser light activation, HNT-PDA nanohybrids were also shown to be activated with other light sources of more practical importance such as a solar simulator, an infrared incandescent lamp and an LED lamp demonstrating their versatility as photothermal

agents. As one of the potential applications of HNT-PDA nanohybrids, their light-activated antibacterial activity was evaluated. The viability of Staphylococcus aureus (*S. aureus*) treated with HNT-PDA nanohybrids was reduced by 6.3 log when irradiated with infrared laser light for 5 min, whereas bacteria not treated with the nanohybrids stayed alive under the same irradiation conditions. Comprising of natural, non-toxic, cost-effective components, HNT-PDA nanohybrids are promising nanoparticles as versatile clay-based photothermal agents that can be utilized in various photo-driven applications.

2.2 Introduction

Photothermal nanoparticles with light-to-heat conversion properties generate heat when irradiated with light. The light energy absorbed by photothermal nanoparticles is emitted via nonradiative decay and results in temperature elevations, which can be remotely controlled via light-activation[98]. The light-activated temperature elevations obtained via photothermal nanoparticles can be uniquely exploited for many different purposes that require remote heating. Although cancer therapy applications of photothermal nanoparticles involving near infrared light-activated destruction of tumors is at the forefront[99], photothermal nanoparticles find many unique applications in the field of materials science such as sterilization of surfaces via heat-killing of bacteria and biofilms[100], sunlight-activated evaporation of water for desalination[101], light-activated self-healing of materials[102,103] or inactivation of viruses on personal protective equipment[104].

Various metals[105–110], carbon-based materials such as carbon nanotubes or graphene oxide[111–114], and organic dyes[115,116] have been demonstrated to present significant light-to-heat conversion properties mainly originating from their plasmonic effect and/or strong near infrared absorption. Semiconducting polymers such as polyaniline, polypyrrole and polydopamine also present strong light-to-heat conversion properties[20, 21]. Specifically, polydopamine, which can be easily coated onto almost any surface due to its unique mussel-inspired adhesive properties[119], can impart photothermal properties to nanoparticles on which it is coated[120–123]. While available photothermal nanoparticles present light-to-heat conversion efficiencies to different extents, depending on the application in which they will be utilized, their toxicity, cost-effectiveness and environmentally friendliness mostly become a concern[124,125]. Considering the wide spectrum of applications where remote heating of nanoparticles can be benefited, new photothermal agents that have strong light-to-heat conversion

properties but are also cost-effective, non-toxic and can be easily integrated into nanocomposite materials are needed.

In this work, halloysite nanotubes (HNTs), which are clay nanoparticles with a hollow tubular structure are imparted photothermal character by simply coating them with photothermal polydopamine to obtain clay-based, natural, non-toxic photothermal nanohybrids with strong light-to-heat conversion properties. HNTs, which have been demonstrated to be important agents of nanotechnology in different applications as drug delivery agents[126–129], nanocarriers for sustained release coatings and films[130–132], electrochemical sensors[133] and reinforcing agents[134–136], have been functionalized with polydopamine before for different purposes including increasing the dispersion stability of HNTs[137], immobilizing enzymes onto HNTs via the polydopamine coating[138], site specific/selective nanofunctionalization[139] or obtaining adsorbents[140,141]. But, in this work, polydopamine coated HNTs (HNT-PDAs) have been systematically studied in terms of their potential as cheap, non-toxic photothermal agents, for the first time. HNTs were functionalized with polydopamine at different concentrations and reaction times and the relationship between polydopamine content on HNTs and the photothermal effect of resulting nanohybrids was investigated. Furthermore, HNT-PDA nanohybrids were demonstrated to be effective photothermal agents that exert significant lethal effect on bacteria by generating high temperature elevations when activated by NIR light.

2.3 Experimental

2.3.1 Chemicals

HNTs were provided by Eczacıbaşı ESAN (Turkey). Dopamine (3-hydroxytyramine hydro- chloride) was purchased from Acros Organics Inc. Ultrapure Tris base (Tris-(hydroxymethyl) aminomethane) was purchased from MP Biomedicals, LLC. Tryptic soy broth (TSB) and agar powder were procured from Medimark (Italy). Deionized (DI) water was used in all experiments.

2.3.2 Preparation of HNT-PDA nanohybrids

An aqueous dispersion of neat HNTs at 10 mg/mL concentration was prepared. HNTs were dispersed in water by ultrasonication (QSonica, Q700, Newtown, CT, USA) for 20 min at 50% amplitude with 5 s pulse on and 2 s pulse off in an ice bath. Dopamine was added to the HNT dispersion at different concentrations (2 mg/mL, 4 mg/mL, 8 mg/mL). The pH was adjusted to 8.5 by adding Tris and the dispersion was stirred vigorously for different reaction times (1 h, 6 h, 24 h) at 30 °C. Following the reaction, the dispersion was centrifuged at 11 000 rpm and the pellet containing the HNT-PDA nanohybrids was washed 6 times using deionized water to remove residual Tris base and unreacted dopamine monomer. Obtained HNT-PDA nanohybrids were dried at 70 °C for 24 h.

Polydopamine (PDA) particles were synthesized as controls. An aqueous dopamine solution at 8 mg/mL concentration and pH 8.5 was stirred vigorously for 24 h at 30 °C until the color of the solution turned dark. The resulting PDA particles were separated

by centrifugation at 11 000 rpm for 10 min and washing 6 times with water followed by drying at 70 °C for 24 h.

2.3.3 Characterization of HNT-PDA nanohybrids

The amount of polydopamine on the HNT-PDA nanohybrids was determined by Thermogravimetric Analysis (TGA) (Shimadzu Corp. DTG-60H (TGA/DTA)). Samples were heated up to 1000 °C at a rate of 10 °C/min under nitrogen flow. The weight percent of polydopamine on each HNT-PDA nanohybrid was calculated by dividing the difference in total weight loss of HNTs and HNT-PDA from 200 °C to 1000 °C by the total weight loss of the PDA control under the same conditions.

Fourier Transform Infrared (FT-IR) analysis of samples was performed with a Nicolet IS10 FT-IR spectrophotometer.

Dynamic light scattering (DLS) measurements of aqueous dispersions of HNT, HNT-PDA and PDA particles were carried out using a Malvern Zetasizer Nano—ZS, (Malvern Instruments Ltd., UK) at 25 °C at a sample concentration of 0.3 mg/mL.

HNT and HNT-PDA nanohybrids in powder form were visualized with Zeiss LEO Supra 35VP scanning electron microscope (SEM). Samples were coated with Au-Pd, and images were taken at 6 kV using the secondary electron detector.

For the transmission electron microscopy (TEM) analysis, samples of HNT and HNT-PDA nanohybrids in powder form were prepared on lacey carbon coated TEM grids. TEM analysis was performed using JEOL JEM ARM200CF operated at 200 kV.

The absorbance spectra of aqueous dispersions of HNTs and HNT-PDA nanohybrids prepared at 5 mg/mL concentration were recorded using Agilent Carry 5000 UV-VIS-NIR Spectrophotometer in the spectral range of 300 to 1000 nm.

2.3.4 Photothermal properties of HNT-PDA nanohybrids

The time-temperature profiles of HNTs and HNT-PDA nanohybrids with different polydopamine contents were constructed under light irradiation by recording the temperatures of the samples. The following light sources and light densities were utilized: i) 808 nm laser module (STEMINC, SMM22808E1200) (Doral, FL USA) at 800 mW/cm^2 (light source was positioned 25 cm away from the sample), ii) near infrared incandescent light bulb (Philips, 250 W Incandescent 230-250V BR125) at 330 mW/cm^2 (light source was positioned 5 cm away from the sample), iii) solar simulator (Oriel, LCS-100) at 3 sun (300 mW/cm^2) (light source was positioned 9 cm away from the sample), iv) full spectrum LED grow lamp at 38 mW/cm^2 (light source was positioned 7 cm away from the sample). 0.2 g HNT or HNT-PDA sample was placed onto a Teflon holder under the light source and temperatures were recorded with a FLIR E6xt thermal camera. For each time-temperature profile, average temperatures and standard error values obtained from three different measurements were reported.

To investigate the photothermal stability and the reusability of HNT-PDA nanohybrids, HNT-PDA $_{(8\ mg/mL)\ 24\ h}$ samples were exposed to 5 consecutive cycles of laser on-off treatments. Samples were exposed to laser light for 2 min, followed by turning off the laser light to allow samples to cool down to room temperature. This cycle was repeated 5 times while the temperature of the sample was continuously recorded with a thermal camera.

2.3.5 Light-activated antibacterial properties of HNT-PDA nanohybrids

S. aureus (ATCC 29213) cells were grown in 3 mL TSB growth medium at 37 °C for 24 h in a shaker incubator at 200 rpm. Grown cells were centrifuged, washed twice with sterile Tris buffer (pH 7.5), and suspended in Tris buffer at a concentration of 10^7 CFU/mL. Aqueous dispersions of HNT-PDA $_{(8\ mg/mL)\ 24\ h}$ and control HNTs were prepared at 20 mg/mL followed by ultrasonication for 20 min at 50% amplitude with 5 s pulse on and 2 s pulse off in an ice bath to eliminate agglomerated particles. 100 µL of the prepared bacterial suspension was added to the wells of a 96 well plate and mixed with 100 µL of the nanohybrid dispersion to obtain test samples or with 100 µL of Tris buffer to obtain control samples lacking the nanohybrids. 2 sets of samples (each sample in triplicate) were prepared. While one set of samples were kept in dark, for the

second set of samples each well was exposed to 808 nm laser light for 2 min and 5 min. All bacterial suspensions (both the ones that were kept in dark and the ones that were irradiated) were serially diluted and plated on TSB agar plates. After the plates were incubated for 24 h at 37 °C, colony counts were performed, and viability was calculated as $\log_{10}$ CFU/mL.

2.4 Result and Discussion

HNTs were imparted photothermal character by the formation of a polydopamine coating on their surfaces. The oxidative polymerization of the dopamine monomer in the presence of neat HNTs allowed the formation of a polydopamine coating on the surface of HNTs (Figure 1a). Following the reaction, the white HNT powder turned into a black-colored powder indicating the successful coating of HNTs with polydopamine and the presence of HNT-PDA nanohybrids (Figure 1b).

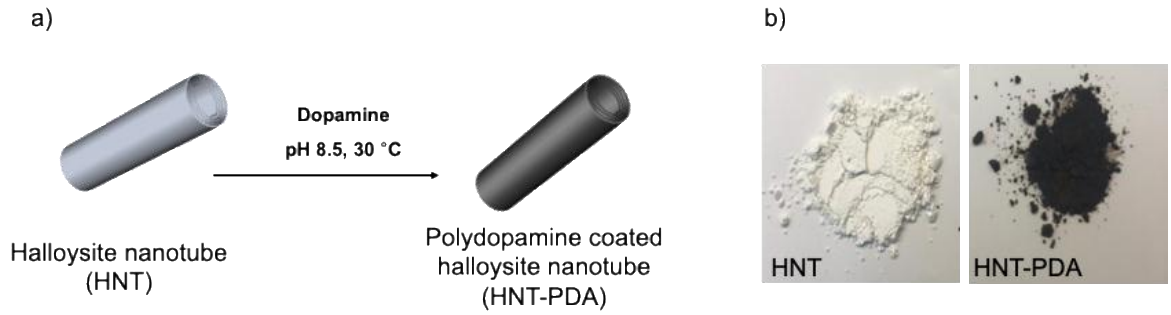

Figure 1. a) Schematic representation of the synthesis of HNT-PDA nanohybrids, b) visual appearance of HNT and HNT-PDA powders.

Table 1. Reaction conditions for the preparation of HNT-PDA nanohybrids.

Sample name	*HNT type*	*Dopamine concentration (mg/mL)*	*Reaction time (h)*
HNT-PDA$_{(2\ mg/mL)\ 1\ h}$	neat	2	1
HNT-PDA$_{(2\ mg/mL)\ 6\ h}$	neat	2	6
HNT-PDA$_{(2\ mg/mL)\ 24\ h}$	neat	2	24
*hydroxy*_HNT-PDA$_{(2mg/mL)\ 24\ h}$	hydroxylated	2	24
HNT-PDA$_{(4\ mg/mL)\ 24\ h}$	neat	4	24
HNT-PDA$_{(8\ mg/mL)\ 24\ h}$	neat	8	24
*hydroxy*_HNT-PDA$_{(8mg/mL)\ 24\ h}$	hydroxylated	8	24

HNT-PDA nanohybrids were prepared at varying dopamine concentration, reaction time and chemical nature of the HNT surface in order to understand whether the amount of the polydopamine coating can be controlled with polydopamine functionalization reaction conditions (Table 1). The polydopamine content of the HNT-PDA nanohybrids was determined by TGA (Figure 2). HNT-PDA nanohybrids presented an additional thermal decomposition starting at 250 °C, coinciding with the decomposition of PDA particles synthesized by self-polymerization of dopamine as controls, which confirms that HNTs were coated with polydopamine. Furthermore, different HNT-PDA nanohybrids prepared at different reaction conditions presented different total weight losses between 200 ºC and 1000 ºC indicating that they have different amounts of polydopamine coating. The weight ratio of the polydopamine to HNT-PDA nanohybrids were calculated as the difference between the total weight loss of HNT-PDA nanohybrids and uncoated HNTs, normalized by the weight loss of PDA particles under the same conditions. As shown in Table 2, the polydopamine content on HNT-PDA nanohybrids varied by the reaction conditions. At constant initial dopamine concentration, the amount of the polydopamine coating on HNT-PDA nanohybrids increased by increasing reaction time. Similarly, increasing the initial dopamine concentration at constant reaction time resulted in larger amounts of polydopamine coating on HNTs. The surface chemistry of HNTs had also significantly affected the yield of the dopamine polymerization. Alkaline treated HNTs (*hydroxy*_HNTs) with increased number of -OH groups on the outer surface were coated with a larger amount of polydopamine relative to neat HNTs under the same reaction conditions. Apparently,

the increased hydrophilic character of *hydroxy*_HNTs facilitated the dopamine polymerization on the HNT surface resulting in larger amount of polydopamine coating. The highest amount of polydopamine coating was obtained when *hydroxy*_HNTs were reacted at 8 mg/mL dopamine concentration for 24 h.

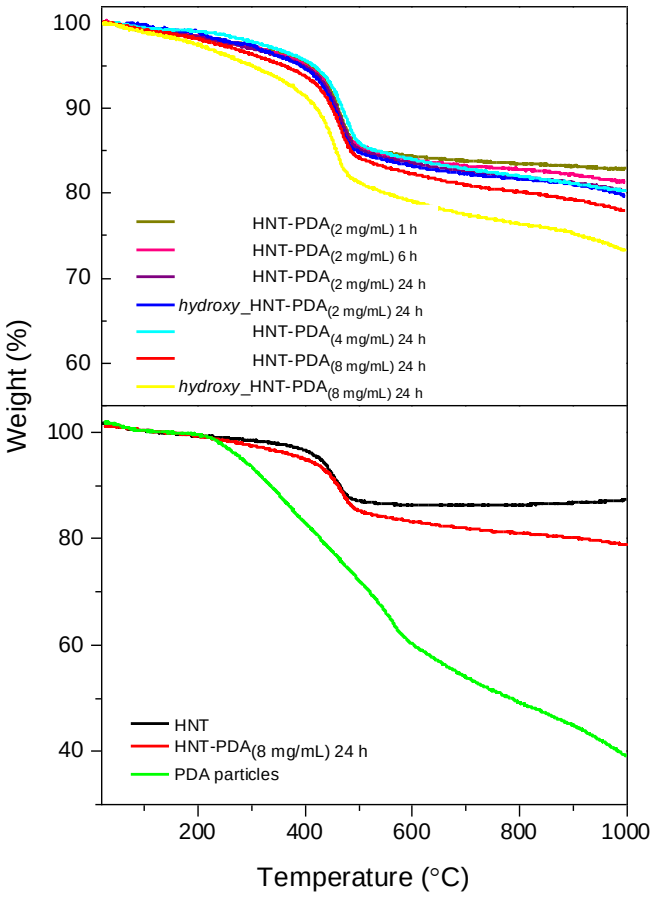

Figure 2. Thermogravimetric analysis of HNTs, HNT-PDA $_{(8\ mg/mL)\ 24\ h}$ nanohybrids and PDA particles, thermogravimetric analysis of HNT-PDA nanohybrids prepared at different reaction conditions.

Table 2**.** The polydopamine content of different HNT-PDA nanohybrids.

Sample name	***Polydopamine coating (wt%)***
HNT-PDA$_{(2\ mg/mL)\ 1\ h}$	**10.0**
HNT-PDA$_{(2\ mg/mL)\ 6\ h}$	**14.5**
HNT-PDA$_{(2\ mg/mL)\ 24\ h}$	**17.10**
*hydroxy*_HNT-PDA$_{(2mg/mL)\ 24\ h}$	**20**
HNT-PDA$_{(4\ mg/mL)\ 24\ h}$	**19.2**
HNT-PDA$_{(8\ mg/mL)\ 24\ h}$	**26.8**
*hydroxy*_HNT-PDA$_{(8mg/mL)\ 24\ h}$	**33.9**

HNT-PDA $_{(8\ mg/mL)\ 24\ h}$ nanohybrids were further investigated in terms of their chemical, physical and optical properties. The presence of the polydopamine coating on HNTs was evidenced by the appearance of new bands at 1613 cm^{-1}, 1494 cm^{-1} and 1296 cm^{-1} on the FTIR spectrum of HNT-PDA nanohybrids corresponding to the -NH bending, aromatic C=C bending and C-N stretching vibrations, respectively (Figure 3a). DLS analysis was performed on aqueous dispersions of HNT-PDA nanohybrids in order to qualitatively compare their length distributions to those from neat uncoated HNTs and control PDA particles (Figure 3b). The size distribution of HNTs at smaller hydrodynamic diameter shifted to a size distribution at larger hydrodynamic diameters indicating that HNT nanoparticles were modified with a polydopamine layer. Furthermore, HNT-PDA $_{(8\ mg/mL)\ 24\ h}$ nanohybrids presented a unimodal size distribution that was completely different than the size distribution of control PDA particles, which were prepared via self-polymerization of dopamine under the same reaction conditions. This result demonstrated that the reaction of dopamine and HNTs resulted only in PDA coated HNTs, and neat PDA particles were not obtained.

Whether the polydopamine coating imparted HNTs with the enhanced absorption properties that are required for NIR light-activated photothermal conversion was studied (Figure 3c). Compared to the neat HNTs, HNT-PDA nanohybrids presented a significantly enhanced, broad absorbance in the UV-VIS-NIR region, potentially due to

the π-π* transition of the benzenoid ring of the PDA backbone[142] indicating that they can be utilized as NIR light-activated photothermal nanoparticles.

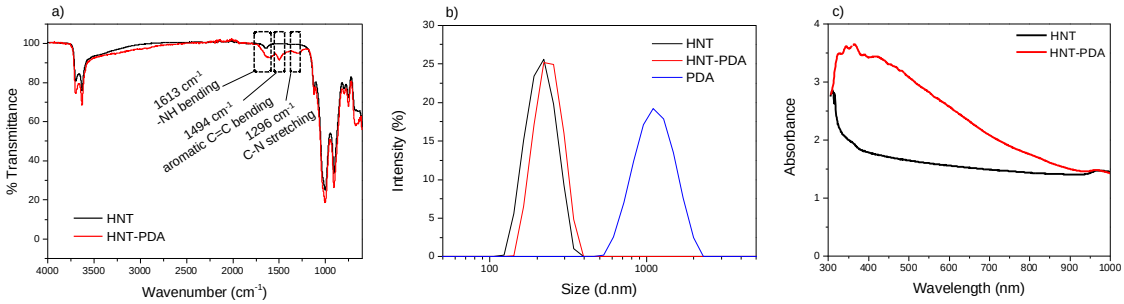

Figure 3. a) FTIR spectra of HNTs and HNT-PDA (8 mg/mL) 24 h nanohybrids, b) DLS analysis of HNTs, HNT-PDA (8 mg/mL) 24 h nanohybrids and PDA particles, c) Absorbance spectra of aqueous dispersion of HNTs and HNT-PDA (8 mg/mL) 24 h nanohybrids.

The polydopamine coating on HNT-PDA nanohybrids was visualized with TEM (Figure 4a). While HNTs preserved their hollow tubular nanostructure following the reaction with dopamine, their smooth surface was shown to become textured indicating the presence of a homogeneously coated polydopamine layer on their outer surface. Furthermore, the hydrophilic polydopamine coating on the HNTs allowed a more homogeneous, agglomeration-free dispersion of HNT-PDA nanohybrids relative to neat HNTs as seen in the SEM images (Figure 4b). A similar result demonstrating the effect of the polydopamine coating on the dispersion stability of HNTs was reported before[137]. Electron microscopy images also confirmed that the dopamine was polymerized on the surface of HNTs rather than self-polymerization, as individual polydopamine particles were not observed.

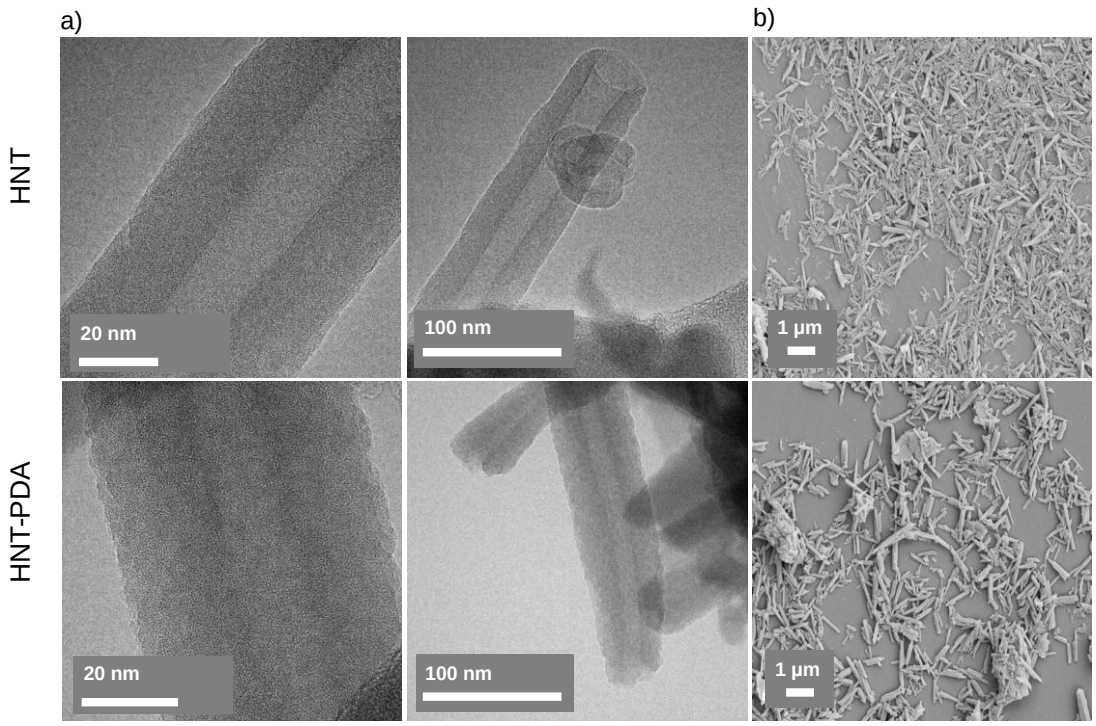

Figure 4**.** a) TEM, b) SEM images of HNT and HNT-PDA $_{(8\ mg/mL)\ 24\ h}$ nanohybrids.

The light-activated heating properties of HNT-PDA nanohybrids were studied by monitoring their temperature under NIR laser light irradiation. Figure 5a demonstrates thermal camera images of HNTs and HNT-PDA $_{(8\ mg/mL)\ 24\ h}$ nanohybrids that have been irradiated with 808 nm laser light for 2 min. While HNT's remained close to room temperature, HNT-PDA nanohybrids in the powder form were heated to 224 °C in only 2 min laser light irradiation due to their photothermal character imparted by the polydopamine coating. Time-temperature profiles of HNT-PDA nanohybrids containing increasing amounts of polydopamine obtained under NIR irradiation are shown in Figure 5b. While the temperature of neat HNTs and *hydroxy*_HNTs without the polydopamine functionalization stayed constant at room temperature when irradiated with NIR laser light for 2 min, the temperature of HNT-PDA nanohybrids with different polydopamine concentrations reached temperatures in the range of 180 °C to 250 °C under the same conditions. The PDA coating turned HNTs into efficient light-to-heat conversion agents, which present significant light-activated temperature elevations of 150-220 °C These NIR laser light-activated temperature elevations obtained from HNT-PDA nanohybrids are comparable to or higher than those obtained from many other

metal-based, carbon-based or organic molecule-based photothermal agents reported in the literature[143]. The degree of light-activated temperature elevations in HNT-PDA nanohybrids was shown to be related to the polydopamine content. As the polydopamine weight ratio in nanohybrids increased, the maximum temperature the nanohybrids can reach upon NIR laser light irradiation has increased. The temperature of the *hydroxy*-HNT-PDA $_{(8\ mg/mL)/24\ h}$ nanohybrids, which had the highest polydopamine content of 33.9 wt.%, has reached an average temperature of 250 °C following a 2 min NIR laser light irradiation. Under the same laser light irradiation conditions neat PDA particles, which were synthesized via self-polymerization of dopamine as controls reached the same temperature as the *hydroxy*-HNT-PDA $_{(8\ mg/mL)/24\ h}$ nanohybrid, demonstrating that the polydopamine functionalization of HNTs have turned them into photothermal clay nanotubes, that present the same photothermal conversion efficiency as neat PDA particles. HNT-PDA nanohybrids were shown to be effective photothermal agents, whose light-to-heat conversion properties and the degree of light-activated temperature elevations can be easily tuned by controlling the amount of the polydopamine content through reaction conditions.

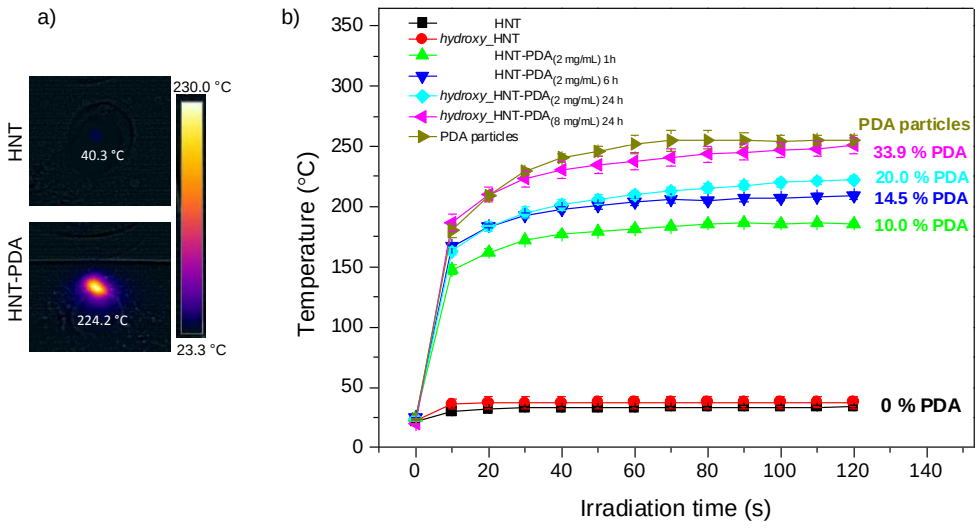

Figure 5. a) Thermal camera images of HNT and HNT-PDA $_{(8\ mg/mL)\ 24\ h}$ nanohybrids in powder form acquired after 2 min 808 nm laser light irradiation, b) Time-temperature profiles of HNT and HNT-PDA nanohybrids with varying polydopamine content under 808 nm laser light irradiation.

The reproducibility of the photothermal effect of HNT-PDA nanohybrids was studied. HNT-PDA nanohybrids, which have been irradiated with laser light for 2 min were allowed to cool to room temperature and re-exposed to laser light. The maximum temperature HNT-PDA nanohybrids can reach upon multiple consecutive irradiation-cooling cycles did not change and HNT-PDA nanohybrids reached the same temperature they have reached in the first cycle by 2 min light activation even after 5 irradiation cycles (Figure 6). This result demonstrated that the HNT-PDA nanohybrids presented a stable photothermal effect and can be re-used in applications where light-activated temperature elevations need to be obtained multiple times.

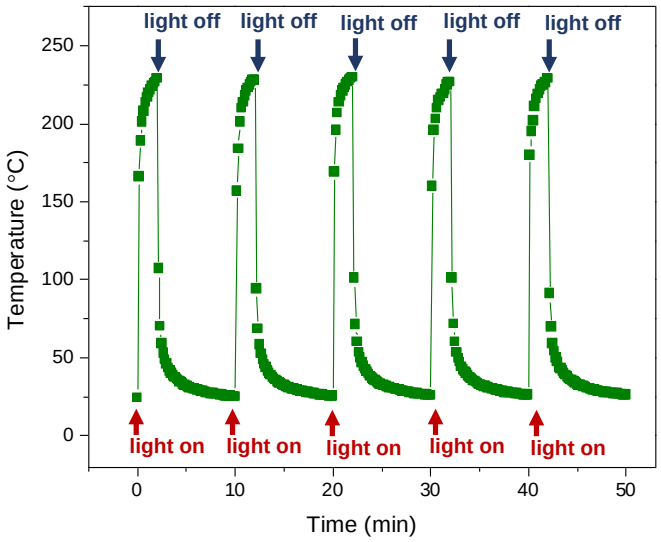

Figure 6. The time temperature profile of HNT-PDA $_{(8\ mg/mL)\ 24\ h}$ nanohybrids constructed under consecutive cycles of 2 min 808 nm laser light irradiation followed by turning the laser light off.

To demonstrate the versatility of HNT-PDA nanohybrids as photothermal nanoparticles in different applications, their photothermal activity under irradiation with different light sources of different light densities was investigated. *hydroxy*_HNT-PDA $_{(8\ mg/mL)\ 24\ h}$ nanohybrids which were shown to have the highest polydopamine content were exposed to different NIR light sources of different nature/different light densities and the light-activated temperature elevations they present were evaluated (Figure 7). A solar simulator, an infrared incandescent light bulb and a full spectrum LED lamp were

used as light sources. When irradiated with sunlight at 3 sun light density HNT-PDA nanohybrids were heated up to 105 °C in 15 min demonstrating that the HNT-PDA nanohybrids were able to present efficient light-to-heat conversion with sunlight as well and can be utilized in various sustainable sunlight-driven applications. A commercial infrared incandescent light bulb was also able to activate the HNT-PDA nanohybrids to generate heat. HNT-PDA nanohybrids were heated up to 102 °C in only 2 min irradiation with the infrared light bulb. While significantly slower, irradiation with a full spectrum LED lamp also led to a significant temperature elevation in HNT-PDA nanohybrids where they were heated up to 50 °C in 1 h. The fact that HNT-PDA nanohybrids have a broad absorption spectrum covering the visible and infrared region due to the polydopamine functionalization makes these nanohybrids absorb light of different wavelengths at different light densities and convert to heat to different extents. Compared to irradiation with laser light, irradiation with a solar simulator, infrared light bulb and a full spectrum LED lamp resulted in higher nonspecific heating of the control HNTs without the polydopamine modification, which can be explained by the broad spectra of the light sources. Nevertheless, the fact that the photothermal effect of the HNT-PDA nanohybrids is not limited to irradiation with laser light and can be activated with many commercial and practical light sources with large illumination areas make the HNT-PDA nanohybrids versatile photothermal agents.

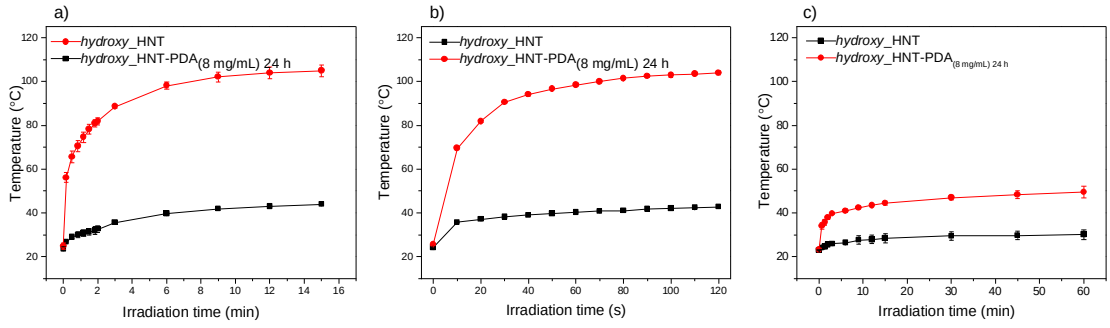

Figure 7. The time-temperature profiles of HNT and HNT-PDA $_{(8\ mg/mL)\ 24\ h}$ nanohybrids constructed under irradiation with a) sunlight, b) light from an infrared incandescent light bulb, c) light from a full spectrum LED grow lamp.

The utilization of photothermal HNT-PDA nanohybrids with light-to-heat conversion properties in light-activated killing of bacteria was studied as one of the many potential applications of these photothermal agents. Viability of *S. aureus* treated with HNT-PDA $_{(8\ mg/mL)\ 24\ h}$ nanohybrids in aqueous suspension was evaluated before and after irradiation with 808 nm laser light (Figure 8). In the presence of HNT-PDA nanohybrids, *S. aureus* were killed by 1.8 log (98.4 %) with irradiation for 2 min, whereas almost all bacteria were killed with a 6.3 log (>99.9999 %) reduction in viability when irradiated for 5 min. Under the same conditions, *S. aureus* that were not treated with HNT-PDA nanohybrids were not affected by the laser light irradiation and stayed alive. Due to the light-activated heat generated by the HNT-PDA nanohybrids, bacteria were exposed to temperatures which allow their hyperthermia related physical destruction[100]. These results have demonstrated that HNT-PDA nanohybrids can be utilized for light-activated elimination of bacteria. Like other photothermal agents, as they offer a heat-based physical bacterial killing mechanism, HNT-PDA nanohybrids are expected to be effective against bacteria that have gained resistance to antibiotics and also other pathogenic microorganisms that are sensitive to temperature elevations such as viruses[144].

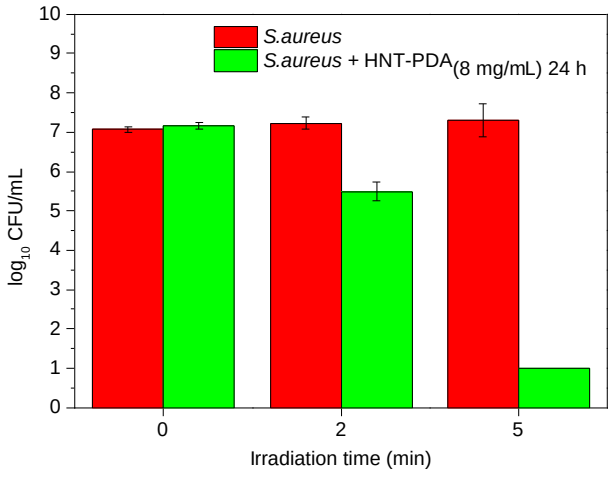

Figure 8**.** Viability of S. aureus treated with HNT-PDA $_{(8\ mg/mL)\ 24\ h}$ under 0 min, 2 min and 5 min irradiation with 808 nm laser light.

2.5 Conclusions

Natural, versatile clay-based nanoparticles, HNTs were converted to effective photothermal agents by simply coating them with polydopamine. The relationship with the polydopamine coating reaction conditions and the polydopamine content of resulting HNT-PDA nanohybrids was determined which allows to control the degree of the photothermal activity and the amount of the light-activated temperature elevations obtained from these nanohybrids. HNT-PDA nanohybrids were shown to be activated with infrared laser light and quickly heated to temperatures ranging from 180 °C to 250 °C in less than 2 min with a photothermal stability over multiple laser on-off cycles. Other light sources with larger illumination areas were also shown to be useful to elevate the temperature of HNT-PDA nanohybrids demonstrating their versatility in different applications. As one of the many potential applications HNT-PDA nanohybrids as light-activated nanoheaters, their ability to kill bacteria under laser light irradiation was demonstrated. Temperature elevations caused by the remote heating of HNT-PDA nanohybrids with light caused physical disruption of *S. aureus* cells. HNT-PDA nanohybrids demonstrated in this work are the first examples of clay based photothermal agents allowing utilization as non-toxic, natural, and cost-effective nanoheaters.

CHAPTER 3. A PHOTOTHERMAL AGENT-BASED COATING FOR AIR FILTERS AND THEIR ANTIBACTERIAL PROPERTIES

3.1 Abstract

Nowadays, air pollution poses a major problem for human health. The bioaerosols that accumulate over time in air filters cause secondary contamination and diseases. For this reason, natural clay-based photothermal agents with strong light-to-heat conversion properties have been incorporated into commercial air filters to create photothermal air filters that can kill retained bacteria when exposed to NIR irradiation. Clay-based photothermal agents prepared by functionalization of HNTs with PDA were dispersed by adding WPU and commercial HEPA filters were coated by spray method. Thanks to the photothermal activity of the HNT-PDA nanohybrids on the filter surface with the applied light, coated filters presented local temperature elevations. The temperature of the HNT-PDA coated filter reached 60°C in 2 min irradiation from an infrared lamp. To study the light-activated antibacterial properties of the HNT-PDA coated HEPA filter, the viability of S. aureus on the coated filter surface was analyzed before and after NIR irradiation. After 20 min of irradiation, the HNT-PDA coated HEPA filter showed 3.4 logs of killing activity. In addition, a *S. aureus* biofilm was formed on the coated filter as a simulation of microorganisms accumulating on the filter surface with a CDC bioreactor, and 2.2 log biofilm killing activity was observed after NIR irradiation for 35 min. The aerosol filtration performance of the filters was tested in the aerosol device

with the organic, inorganic, and bioaerosol particles in the indoor air. The filtration efficiency (ŋ, %), quality factor (QF), and pressure of HNT-PDA coated HEPA filters were calculated, and it was demonstrated that the coating nanohybrids did not negatively affect the filtration properties. The light-activated HNT-PDA coated HEPA filter was analyzed before and after NIR irradiation to analyze the killing activity of the *S. Aureu*s bioaerosol. After 20 min of irradiation, killing activity was observed in HNT-PDA coated HEPA filter 5.5 log. A new approach to antibacterial filtration systems has been realized by incorporating non-toxic, light-activated photothermal clay-based nanohybrids into the commercial air filter.

3.2 Introduction

In the last few years, the decline in indoor air quality has significantly reduced the quality of life for many people. Hence, the impact of air pollution on health has begun to raise concerns[145]. Research studies have reported that exposure to accumulated airborne bacterial microorganisms and other particles causes various diseases such as allergies, asthma, cardiovascular diseases, Legionnaire's disease and sick building syndrome [146–149]. Especially in heating, cooling, and air conditioning systems, microorganisms captured on air filters may grow on the air filter surface and their rapid spread to the indoor environment constitutes an important source of secondary microbial contamination[150].

In this view, numerous studies have focused on improving air quality via development of air filters for bioaerosol removal[151–154]. The most commonly used technique is the mechanical filtration method which is based on simply capturing and retaining air pollutant particles [155]. There are different types of filters depending on the particle size and area of use. The most common is the high efficiency particulate air filtration (HEPA) media. HEPA filters have high efficiency, removing 99.95% of particles with a diameter of 0.3 μm and larger with a pressure drop of 25–50 mmAq [156,157]. However, there is no contribution to preventing accumulated microorganisms from causing secondary contamination on the filter surface.

There are other air cleaner systems aiming to decrease bioaerosol related air pollution based on adsorption, ozonation[158–160], ultraviolet germicidal irradiation[161], photocatalysis[162,163], and electrostatic precipitator with ionization[164]. Although these technologies remove bioaerosol particles from the air, they may have a detrimental impact on human health and the environment because of disadvantages such as unhealthy UV irradiation and ozone, toxic and decomposition products, heavy hazardous particles, and pollutant emission products[155,159,165]. Alternatively,

antimicrobial agents have been incorporated into air filters for bioaerosol removal and deactivation of retained microorganisms [154].

Metal nanoparticles and carbon nanotubes (CNTs) as antibacterial agents have been demonstrated to be incorporated into air filtration systems resulting in antibacterial air filters, which allow elimination of microorganisms from the filter surface [151,152,166,167]. But the fact that contact and exposure of nanoparticles causes health problems such as skin irritation, mucosal inflammation and necrosis [153,166,168] raises concerns on the use of antibacterial air filters containing metal nanoparticles.

Alternatively, some plant extracts such as Melaleuca alternifolia (tea tree)[169], Eucalyptus[170] and Sophora flavescens[171] have begun to be used promisingly as natural antibacterial agents in in air filters[172,173]. It has been observed that an antimicrobial air filter coated with tea tree oil has inactivated 99% of the bacterial aerosol while organic antimicrobial agents are harmless to human health with their less toxic content compared to inorganic materials[153,174]. However, the satisfactory antibacterial properties of plant extracts may decrease by external factors such as humidity and temperature [166].

The ideal air filter medium to be used for bioaerosol removal should not only have effective filtration properties, but also needs to be cost-effective, non-toxic, harmless for human health, reusable, and most notably should be able to deactivate microorganisms accumulated on the filter surface. In this study, commercial air filters were coated with photothermal nanohybrids obtained by functionalizing natural halloysite nanotubes (HNTs) with polydopamine (PDA) to develop light-activated antibacterial air filters. The antibacterial properties of HNT-PDA photothermal nanohybrids have been demonstrated in previous studies[175]. Here, a novel antibacterial air filter that physically inactivates microorganisms accumulated on the filter surface, was obtained by coating commercial HEPA filters with HNT-PDA nanohybrids. HNT-PDA nanohybrids were coated on the filter surface using the spray-coating method, and bioaerosol filtration properties and the light-activated antibacterial activity of the resulting air filters were presented.

3.3 Experimental

3.3.1 Chemicals

HNTs were provided by Eczacıbaşı ESAN (Turkey). Dopamine (3-hydroxytyramine hydrochloride) was purchased from Acros Organics Inc. Ultrapure Tris base (Tris-(hydroxymethyl)- aminomethane) was purchased from MP Biomedicals, LLC. Triton X-100 for analysis was purchased from Merck Company. Tryptic soy broth (TSB) and agar powder were procured from Medimark (Italy). The model organic aerosol Bis(2-ethylhexyl) sebacate ≥ 97.0 % (GC) was obtained from Aldrich Chemistry, while the model inorganic aerosol Sodium Chloride was obtained from Sigma Aldrich. Deionized (DI) water was used in all experiments. Commercial HEPA-13 (H13) air filters were provided by Fersan Vac Bag Industry. Anionic, aqueous polyurethane (WPU) dispersion based on a polyester–polyol was kindly supplied by Punova R&D and Chemicals Inc. (Turkey) with a 30 wt % solid content.

3.3.2 Preparation of the HNT-PDA nanohybrids

An aqueous dispersion of pure HNTs at a concentration of 10 mg/mL was prepared. After the HNTs were dispersed in water by ultrasonication (QSonica, Q700, Newtown, CT, USA) for 20 min with 5 s pulse on and 2 s pulse at 50% amplitude in an ice bath, then dopamine was added to the HNT dispersion at a concentration of 8 mg/mL. The pH was adjusted to 8.5 by adding Tris (Tris-(hydroxymethyl) aminomethane)) and the dispersion was stirred vigorously for 24 h at room temperature. After the reaction, the dispersion was centrifuged at 11,000 rpm and the pellet containing the HNT-PDA nanohybrids was washed several times with deionized water to remove any residual

Tris base and unreacted dopamine monomer. The resulting HNT-PDA nanohybrids were dried at 70 °C for 24 hours.[175].

3.3.3 Preparation of the WPU/HNT-PDA dispersion for spray-coating

To prevent agglomeration and precipitation of the HNT-PDA nanohybrids, an aqueous dispersion of HNT-PDA in 5% Triton X-100 at a concentration of 0.16 g/mL was prepared. The dispersion was ultrasonicated (QSonica, Q700, Newtown, CT, USA) for 20 min at 50% amplitude with 5 s pulse on and 2 s pulse off in an ice bath. Then, the WPU dispersion (30 wt % solids) was added to the HNT-PDA dispersion resulting in a HNT-PDA concentration of 0.05 g/mL.

3.3.4 Spray-coating of the HEPA filter

The airbrush for spray coating (Magicbrush Airbrush Kit Ab-101a) was set up in a chemical hood by adjusting the air pressure to 15-35 psi. Prepared HNT-PDA dispersion was placed in the chamber of the airbrush and sprayed onto the HEPA filter by hand. The spray-coated filter was dried at room temperature.

3.3.5 Characterization of the HNT-PDA coated HEPA filters

The amount of HNT-PDA on the coated HEPA filter was determined by Thermogravimetric Analysis (TGA) (Shimadzu Corp. DTG-60H (TGA/DTA)). Under nitrogen flow, samples were heated to 1000 °C at a rate of 10 °C/min. The weight percent of the HNT-PDA nanohybrids on each coated HEPA filter was calculated by finding the difference in total weight loss of neat HEPA 13 filter and HNT-PDA nanohybrids from 200 °C to 1000 °C and normalizing this difference by the remaining weight of the HNT-PDA nanohybrids under the same conditions. To determine the stability of the HNT-PDA coated filters isothermal TGA was applied by keeping the

samples at 180°C for 1 h under nitrogen flow and monitoring the weight loss due to any potential decomposition.

HNT-PDA coated HEPA filters were visualized with Zeiss LEO Supra 35VP scanning electron microscope (SEM). Samples were coated with Au-Pd, and images were taken at 6 kV using the secondary electron detector.

3.3.6 Photothermal properties of HNT-PDA nanohybrids

Time-temperature profiles of the HNT-PDA coated HEPA filters were constructed under NIR irradiation from a 100W Infrared UVA+UVB3 Full Spectrum Animal & Plant Growth light source (General Electric) was used with a light intensity of 100 mW/cm^2 and from a 808 nm laser module (STEMINC, SMM22808E1200) (Doral, FL USA) at 800 mW/cm^2 light density by recording the temperature of the samples with a FLIR E6xt thermal camera. For each time-temperature profile, coated and neat filters were exposed to NIR light for 2 min and their measurements were taken with thermal camera temperatures were recorded. Mean temperature and standard error values of three different measurements were reported.

To determine the stability of the HNT-PDA surface coating on the filters, time-temperature profiles of the coated samples under NIR irradiation were constructed before and after washing in water. Samples that were dipped in water for 2 min and dried were irradiated with NIR light and temperatures were monitored with the thermal camera.

To determine the stability of the HNT-PDA surface coating on the filters, time-temperature profiles of the coated samples under NIR irradiation were constructed before and after exposing the filters to air flow. Samples that were exposed to air flow from a pressurized airline 15 psi for 30 min were irradiated with NIR light and temperatures were monitored with the thermal camera.

3.3.7 Light-activated antibacterial properties of the HNT-PDA coated filters

S. aureus (ATCC 29213) cells were grown in 3 mL of TSB growth medium at 37 °C for 24 h in a shaker incubator at 200 rpm. After centrifugation, the growing cells were washed twice with sterile Tris buffer (pH 7.5) and suspended in Tris buffer at a concentration of 10^7 CFU/mL. 200 μL of the prepared bacterial suspension was dropped onto 1 cm x 1.5 cm HNT-PDA coated and neat filters. For each filter two sample sets were prepared while one sample set was kept in the dark, the second sample set (each sample in triplicate) was exposed to 100 mW/cm^2 (General Electric 100W Infrared UVA+UVB3 Full Spectrum Animal & Plant Growth Light) for 10 and 20 min. Following the NIR irradiation each sample was added into 400 μL of Tris buffer and vortexed to transfer all bacteria into the buffer. All bacterial suspensions (both the ones that were irradiated and the ones that were kept in dark) were serially diluted and plated on TSB agar plates. Plates were incubated at 37 °C for 24 h and viability was calculated as $\log_{10}$ CFU/mL by counting colonies.

3.3.8 Antibiofilm properties of the HNT-PDA coated HEPA filters

The CDC bioreactor (Biosurfce Technologies, CBR 90 Standard) was used to grow *S. aureus* (ATCC 29213) biofilms on the HNT-PDA coated and neat HEPA filter surfaces for 48 hours. *S. aureus* cells were grown in 3 mL of TSB growth medium at 37 °C in a shaker incubator at 200 rpm for 24 h. TSB growth medium was prepared in two different concentrations; 350 ml batch phase (30 g/L) and 20 L continuous phase (1.5 g/L). After the CDC reactor and prepared TSB media were autoclaved, 2 cm x 2 cm coated, and neat filters were mounted in the coupon holders inside the CDC reactor in a sterile hood. 350 mL batch phase was transferred into the reactor in the sterilization environment using a burner flame and the reactor outlet line was clamped. *S. aureus* cells at a concentration of 10^8 CFU/mL were inoculated into the reactor. The completed assembly was incubated at 37 °C for 24 hours with stirring (120 rpm). After this batch phase growth, the effluent line was opened, and the reactor medium was constantly renewed at 11.70 mL/min 12.54 rpm for 24h. The samples were aseptically removed from the reactor and placed on a Teflon plate. The set of the coated and neat filter

samples (each sample in triplicate) were prepared. While one set of samples were kept in the dark, the second set of samples were exposed to NIR light (Infrared UVA+UVB3 Full Spectrum Animal & Plant Growth Light (100 mW/cm^2) for 35 min. All samples were transferred into 10 mL Tris base. Bacterial suspensions were serially diluted and plated on TSB agar plates. The plates were incubated for 24 h at 37 °C, colonies were counted, and viability was calculated as $\log_{10}$ CFU/mL.

For imaging, the biofilms on the filters were fixed with 1.5 mL glutaraldehyde (2.5%). After 2 h, the samples were washed with Tris base and kept in ethanol solutions of 30, 50, 70, and 100 % for 5 min. The samples were transferred to a petri dish and left to dry at room temperature. Then, the biofilm on the filter surface was visualized with Zeiss LEO Supra 35VP scanning electron microscope (SEM).

3.3.9 Bioaerosol removal and deactivation properties of HNT-PDA coated HEPA filters

Following to the exposure of the air filters to 50 min of *S. aureus* aerosol flow in the air filter test system, filters were aseptically removed from the test module and irradiated with NIR light for 20 min. Bioaerosol particles retained on the surface of all filter samples (before and after irradiation) were transferred to 20 mL Tris buffer and vortexed vigorously. Bacterial suspensions were serially diluted, and bacteria plated on TSB agar plates were incubated at 37 °C for 24 h. Colony counts were made, and viability was calculated as $\log_{10}$ CFU/mL.

3.3.10 Air filtration performance of the HNT-PDA coated HEPA filters

The air filtration performance of the HNT-PDA coated HEPA filters were determined by using aerosols of neutralized charged monodisperse solid NaCl (0.5 g/mL), DEHS in ethanol (solvent) (1 g/mL) and *S. aureus* cells in Tris buffer (10^8 CFU/mL) were used as models for inorganic, organic and bioaerosols, respectively. The custom-made filtration test system included an aerosol generator (TSI, Six-Jet Atomizer 9306)

connected to pressured air line (Fairchild, 30252 Model 30 Precision Regulator), a diffusion dryer (TSI, Diffusion Dryer 3062-NC) an optical sizer (TSI, Optical Particle Sizer (OPS) 3330), a differential pressure gauge, a laminar flow meter and a stainless steel filter module (**Hata! Başvuru kaynağı bulunamadı.**).

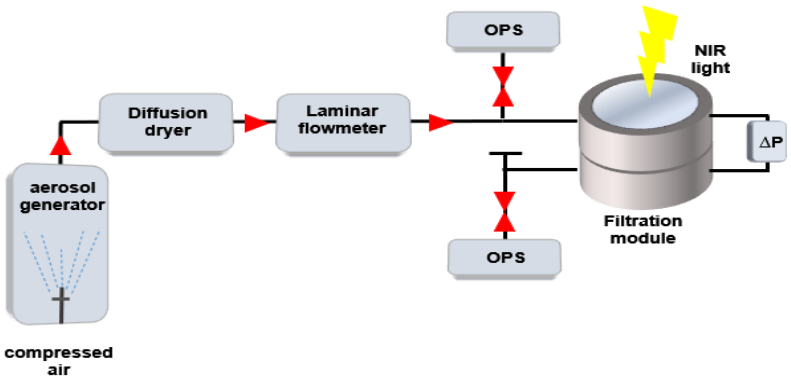

Figure 9. Filtration test system

Aerosols were generated at an airflow of 0.5 L/min and 0.02 m/s velocity for 50 min. While the pressure drop was recorded with the manometers at the inlet and outlet of the filter system, the particle numbers were measured with the particle sizer. The quality factor (QF) was calculated and tabulated by measuring the filtration efficiency (ŋ, %) and the pressure drop with Eq.1

$$ŋ(\%) = 1 - \frac{C_{outer}}{C_{inner}} \qquad \text{Eq. 1}$$

$$QF(Pa^{-1}) = \frac{-\ln(1-ŋ}{\Delta P} \qquad \text{Eq. 2}$$

3.4 Result and Discussion

To obtain photothermal air filters, which can kill captured bacteria upon NIR irradiation, natural clay-based photothermal agents with strong light-to-heat conversion properties were incorporated into commercial air filters. Clay-based photothermal agents were prepared by functionalizing HNTs with PDA,[175] resulting in HNT-PDA nanohybrids with excellent light-activated heating properties. To obtain an optimal coating dispersion, that allows homogeneous coating of HNT-PDA nanohybrids on the air filter with minimal agglomerations, HNT-PDA nanohybrids were dispersed in aqueous solutions containing varying amounts of a surfactant. Furthermore, to obtain a stable coating on the air filter, that is not removed by washing or airflow, the coating dispersion also contained waterborne polyurethane (WPU) that was expected to act as an adhesive that fixes the HNT-PDA nanohybrids on the filter surface. Variations of HNT-PDA, surfactant and WPU concentrations, that were used in the coating dispersion were presented in Table 3. The commercial HEPA filter was spray-coated with the coating dispersion prepared using an airbrush and air dried (Figure 10a). The color of the spray-coated filter surface changed from white to black, demonstrated that the black-colored HNT-PDA nanohybrids were homogeneously coated on the filter surface (Figure 10b).

Table 3. Content of the coating dispersions

Sample	HNT-PDA (g/mL)	WPU (g/mL)	Triton (v/v%)
1	0,1	-	3
2			5
3	0.16	-	3
4			5
5	0.16	0.001	5
6		0.02	
7		0.05	

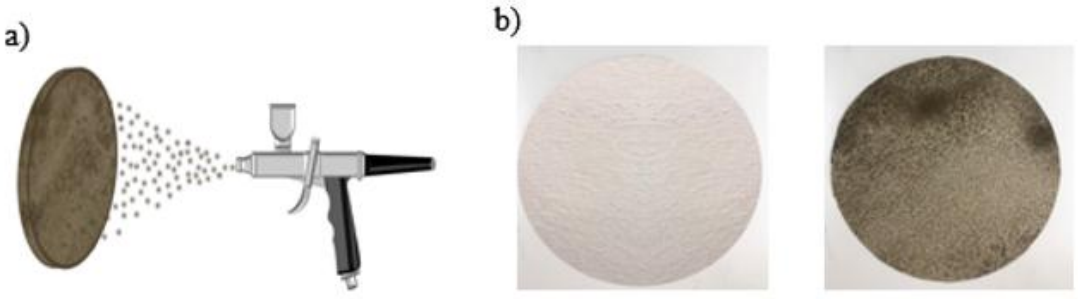

Figure 10. (a) Spray-coating of the HEPA filter with HNT-PDA nanohybrids, (b) visual appearance of neat and HNT-PDA coated HEPA filters.

Light-activated heating properties of the HNT-PDA coated HEPA filters were studied under irradiation from a NIR incandescent bulb to understand whether the coated filters can be heated to temperatures that suffice the physical killing of the surface-attached bacteria (Figure 11). While neat HEPA filters did not heat up under 2 min NIR irradiation, filters coated with HNT-PDA dispersions at a concentration of 0.1, 0.16 g/mL presented temperature elevations of 20 to 30 ℃. This result demonstrated that the HN-PDA coating on the filter has imparted the HEPA filter with photothermal properties. The concentration of the surfactant or the WPU in the coating dispersion was demonstrated not to effect the light-to-heat conversion properties of the coated filters.

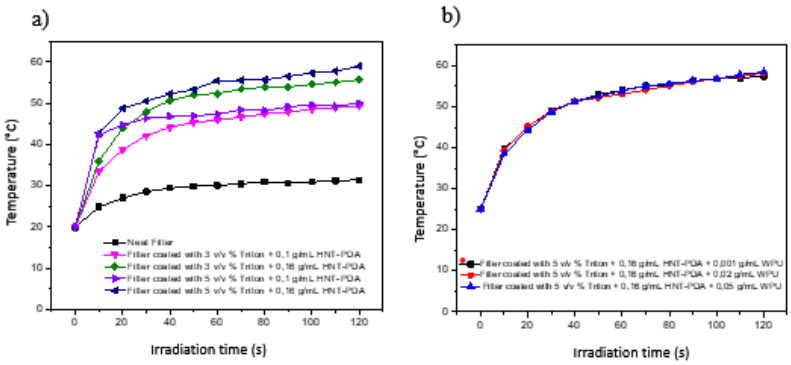

Figure 11. (a) Time-temperature profiles of neat and HNT-PDA coated HEPA filters with varying surfactant and HNT-PDA concentrations under NIR irradiation at 100 mW/cm^2 light density. (b) Time-temperature profiles HEPA filters coated with dispersions containing varying WPU concentrations under NIR irradiation at 100 mW/cm^2.

HNT-PDA coated HEPA filters were visualized by SEM (Figure 12a). The images have shown that the fibers in the control neat filter have a reticulated structure, and when successfully coated with photothermal HNT-PDA nanohybrids, its structure became relatively rough but did not deform. To analyze the amount of HNT-PDA nanohybrids present on the filter surface, neat and coated HEPA filters were tested with TGA. The difference in weight loss of both samples between 200 and 1000 ℃ demonstrated that the coated filter contained 27.56 wt % HNT-PDA nanohybrids (Figure 12b). Isothermal TGA (Figure 12c) of the HNT-PDA coated filters allowed to understand whether the temperature increases due to the HN-PDA photothermal agents included in the filters would cause any decomposition of the filter. The weight of the coated air filters remained constant at 180 °C for 1 hour, demonstrating that there was no decomposition in the structure of the filter at high temperatures.

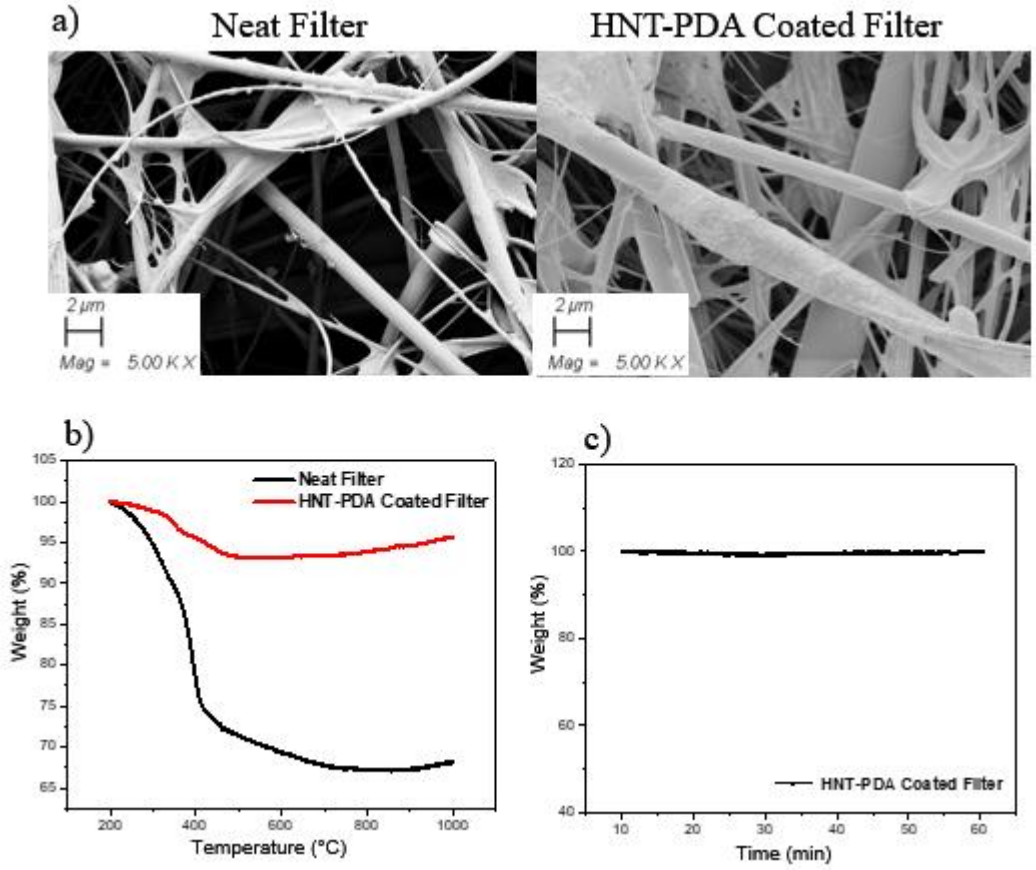

Figure 12. (a) SEM images of neat and HNT-PDA coated HEPA filters, (b) TGA of neat and HNT-PDA coated HEPA filters, (c)Isothermal TGA of HNT-PDA coated HEPA filter.

The light-activated heating properties of the HNT-PDA coated filters were also investigated under NIR laser light irradiation. Figure 13 shows the time-temperature graphs of the neat HEPA filter and the HNT-PDA coated HEPA filter irradiated with 808 nm laser light for 2 min. While there was no temperature increase in the uncoated control filter, the coated HEPA filters were heated to 173°C by laser irradiation for 2 min because of their photothermal properties. This result demonstrated that with irradiation from different light sources at different light densities, different light-activated temperature elevations can be obtained, which would allow utilization of these coatings for different applications requiring different temperature elevations.

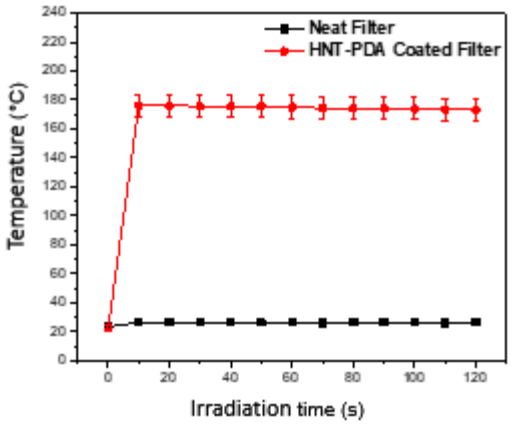

Figure 13. The time-temperature profiles of neat and HNT-PDA coated HEPA filters under irradiation with a 808 nm laser module at 800 mW/cm^2 light density.

The resistance of the HNT-PDA coated filters to environmental factors was analyzed. As shown in Figure 14, the photothermal profiles of the coated filters were obtained before/after the filters were rinsed with water and before/after the filters were exposed to air flow to determine whether the photothermal coating remained on the filter under these conditions. The effective temperature increase of the HNT-PDA coated filter under laser light irradiation was monitored for 2 min. The measurement was repeated under the same conditions after the coated filter was rinsed and dried (Figure 14a). The fact that the same temperature elevations were obtained after the rinse showed that the nanohybrids on the filter surface did not break off after rinsing and adhered to the filter surface perfectly. Similarly, after 30 min exposure to nitrogen gas flow, the same temperature elevations as the untreated filter was obtained (Figure 14b) demonstrating that the HNT-PDA nanohybrids and their photothermal properties remained stable.

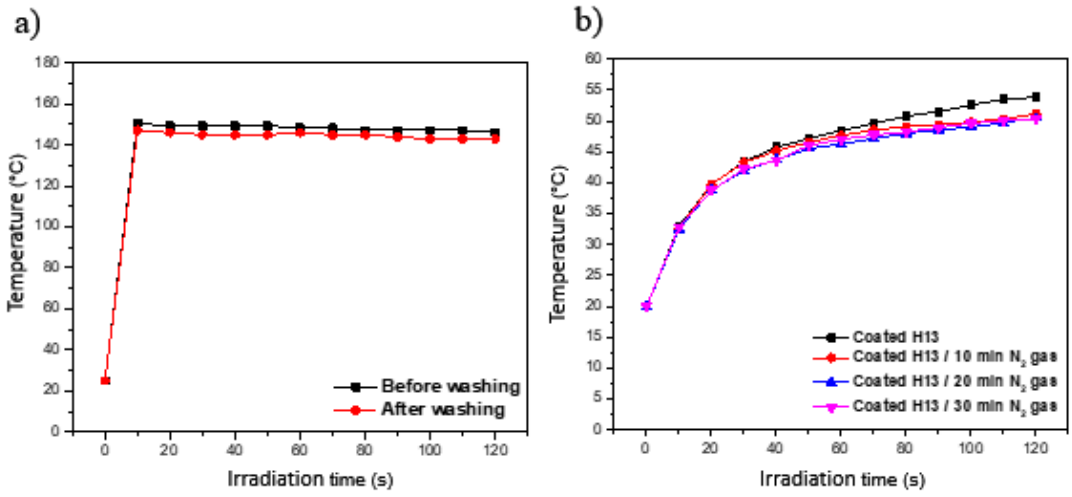

Figure 14. Time-temperature profiles of the HNT-PDA coated HEPA filter before and after a) rinsing with water b) exposure nitrogen flow for 30 min.

To study the light-activated antibacterial properties of the HNT-PDA coated HEPA filters, the viability of *S. aureus* on the surface of these filters was evaluated before and after NIR irradiation for 10 and 20 min (Figure 15). When the HNT-PDA coated HEPA filters were irradiated for 10 min, a 0.5 log decrease was observed in the viability of *S. aureus*, while a 3.4 log decrease in the viability of the bacteria was observed when irradiated for 20 min. Under the same conditions, control filters without photothermal nanohybrids were not affected by NIR lamp irradiation, and there was no change in *S. aureus* viability. The results showed that commercial air filters coated with photothermal nanohybrids physically killed bacteria by light and the HNT-PDA coating converted commercial HEPA filters to light-activated antibacterial air filters.

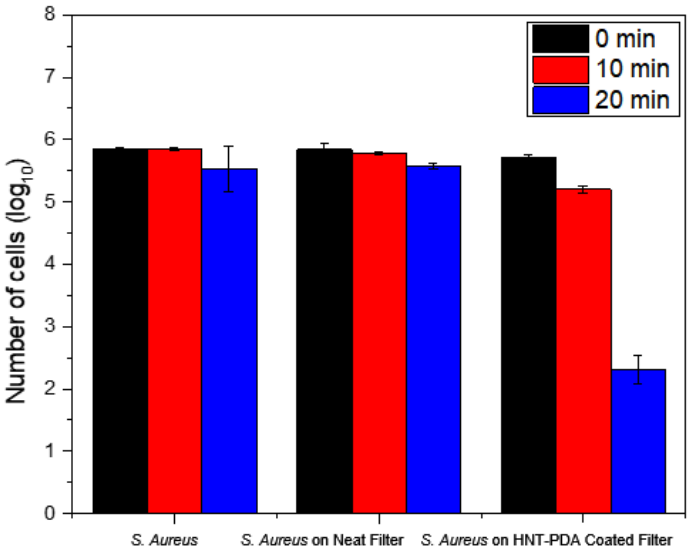

-

Figure 15. Viability of *S. aureus* dropped on neat, and HNT-PDA coated filters treated with NIR light for 0, 10, and 20 min.

The coating of photothermal nanohybrids with light-activated properties on commercial air filters provided an effective solution for eradicating biofilms as well. Dynamic *S. aureus* biofilms were established on the surface of filters (neat and HNT-PDA coated HEPA filters) by using a CDC bioreactor and visualized with SEM images. (Figure 16a). The number of viable cells in the biofilm was determined before and after 35 min NIR irradiation. In HNT-PDA coated filters a 2.2 log reduction in the number of viable cells was observed after the NIR lamp irradiation (Figure 16b). For neat filters without nanohybrids, the viability of *S. aureus* biofilm after light irradiation under the same condition did not change. Hence, an important solution has been provided to a problem in the field of air filtration, which is that accumulated microorganisms retain on the filter surface and form biofilms. The photothermal HNT-PDA coating imparted light-activated antibiofilm properties to air commercial air filters.

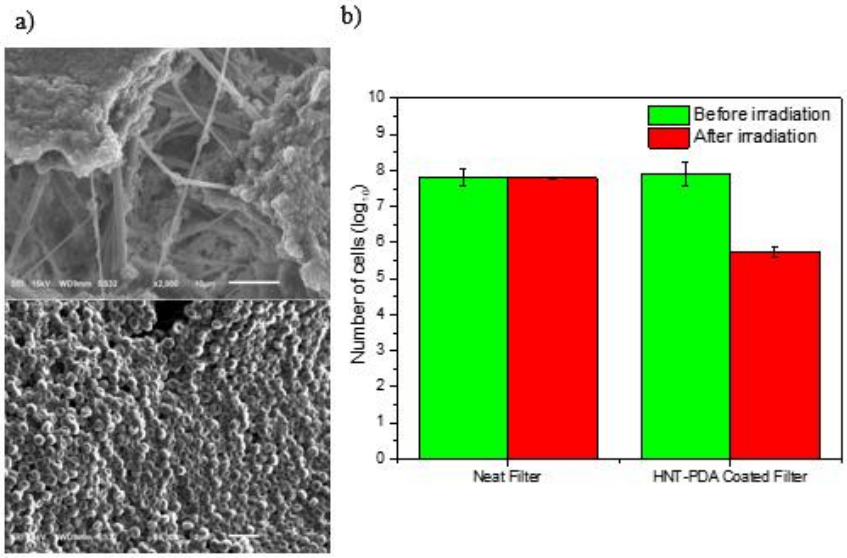

Figure 16. (a) SEM images of biofilm on the filter surface (b) Viability of *S. aureus* biofilm established on neat and HNT-PDA coated HEPA filters after 0 and 35 min NIR irradiation.

The effect of the HNT-PDA coating on the filtration performance of a commercial HEPA filter was studied by using a custom-made air filtration test system (Table 4). Aerosols of NaCl, DEHS and *S. aureus* were generated with an aerosol generator as model inorganic, organic and bio aerosols, respectively. The filters were exposed to aerosol flow at 0.5 L/min flow rate for 50 min, and the filtration efficiency (ŋ, %) was calculated by measuring the inlet and outlet particle numbers with an OPS. In addition, the upstream and downstream pressure difference (ΔP) was measured, and the quality factor (QF) was calculated. For the organic and inorganic aerosol, the pressure difference of the coated HEPA filter samples is 60 Pa, and the quality factors are calculated as 0.11 Pa^{-1}, showing the same value as the neat HEPA filter. The HNT-PDA coating did not have a negative impact of the permeability of the filter. The filtration efficiency of coated HEPA filters was above 99.90% for organic and inorganic aerosol particles and when compared to neat filters a decrease in filtration efficiency was not observed. Furthermore, when the filters were tested with *S. aureus* bioaerosol, the pressure difference remained constant at 60 Pa and the filtration efficiency was 99.99%. Based on these values, the quality factor of the coated HEPA filter was 0.12 Pa^{-1}. As a result, it can be concluded that the filtration performance of the commercial air filters

was not negatively affected by the HNT-PDA coating and the prepared light-activated antibacterial/antibiofilm air filters presented excellent filtration performance.

Table 4. Filtration performance of neat and HNT-PDA coated HEPA filters.

	Sample name	Concentration down stream (# / cm³)	Concentration up stream (# / cm³)	η (%)	ΔP (Pa)	QF (Pa-1)
Inorganic Aerosol (NaCl)	HNT-PDA Coated Filter	2646	2.114	99.9204	60	0.11
	Neat Filter	3322	1.340	99.9596	60	0.11
Organic Aerosol (DEHS)	HNT-PDA Coated Filter	4337	4,276	99.9013	60	0.11
	Neat Filter	4576	3,521	99.9014	60	0.11
Bacterial Aerosol (S. Aureus)	HNT-PDA Coated Filter	4129	0,322	99.9922	60	0.12
	Neat Filter	3402	0,748	99.9780	60	0.12

Whether the bacteria retained on the HNT-PDA coated filters following *S. aureus* aerosol flow can be killed by light activation was studied. After the HNT-PDA coated filters were exposed to *S. aureus* flow for 50 min, filters were removed from the test module and irradiated with the NIR light with 100 mW/cm^2 light density for 20 min. It was observed that the HNT-PDA coated HEPA filters killed almost all of the 10^6 *S. aureus* bacteria retained on the filter via light-activated heating (Figure 17). Under the same conditions approximately 10^6 *S. aureus* cells retained on the neat HEPA filters remained alive after light irradiation, as there was no change in the number of cells.

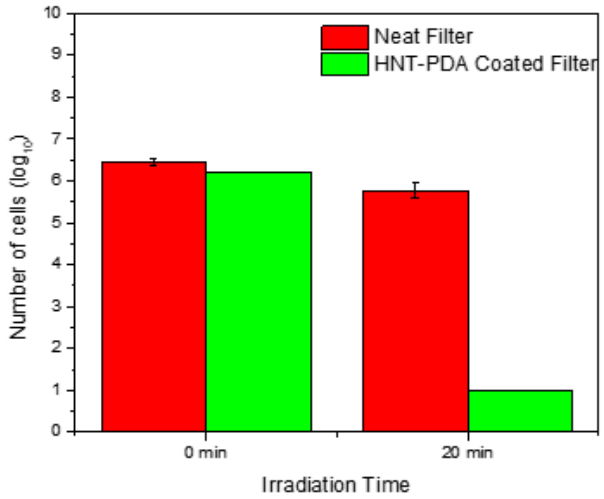

Figure 17. Viability of *S. aureus* cells retained on the neat and HNT-PDA coated HEPA filters before and after 20 min NIR irradiation.

3.5 Conclusions

Photothermal HNT-PDA nanohybrids were successfully coated onto commercial HEPA filters via spray-coating resulting in light-activated antibacterial air filters. Strong photothermal effect, uniformity and stability was achieved by optimizing the concentration of the HNT-PDA nanohybrids, surfactant and WPU in the coating dispersion. HNT-PDA coated HEPA filters were demonstrated to heat up to 60 °C and 173 °C upon 2 min irradiation with a NIR laser and c, respectively. The light-activated temperature elevations of the coating applied to HEPA filters has provided a solution to indoor air pollution that adversely affects human health by microorganisms remaining and growing on the filter surface. The coated HEPA filters were activated with an 808 nm laser module for 20 min, and it was observed that the bacteria in contact with the filters were killed with a reduction of 3.4 log. In addition, the eradication of biofilm accumulated in the HNT-PDA coated filters by light was investigated by forming a dynamic *S. aureus* biofilm on the filter surface. The temperature elevations of the filters upon 35 min NIR irradiation removed the biofilm with a 2.2 log reduction in the number of viable bacteria. The HNT-PDA coated filters were shown to present similar aerosol filtration performance as the neat filters demonstrating that the coating did not adversely affect the filtration performance. Following a *S. aureus* bioaerosol, all of the bacteria retained on the filter were killed by NIR irradiation. In this study, antibacterial air filters that improve indoor air quality have been obtained via a new approach by integrating the excellent photothermal properties of the non-toxic, natural, and cost-effective HNT-PDA nanohybrids into commercial air filter.

REFERENCES

(1) Yang, J.; Choi, J.; Bang, D.; Kim, E.; Lim, E.-K.; Park, H.; Suh, J.-S.; Lee, K.; Yoo, K.-H.; Kim, E.-K.; Huh, Y.-M.; Haam, S. Convertible Organic Nanoparticles for Near-Infrared Photothermal Ablation of Cancer Cells. *Angew. Chemie* **2011**, *123* (2), 461–464. https://doi.org/10.1002/ange.201005075.

(2) Zhang, L.; Tang, B.; Wu, J.; Li, R.; Wang, P. Hydrophobic Light-to-Heat Conversion Membranes with Self-Healing Ability for Interfacial Solar Heating. *Adv. Mater.* **2015**, *27* (33), 4889–4894. https://doi.org/10.1002/adma.201502362.

(3) He, F.; Han, M.; Zhang, J.; Wang, Z.; Wu, X.; Zhou, Y.; Jiang, L.; Peng, S.; Li, Y. A Simple, Mild and Versatile Method for Preparation of Photothermal Woods toward Highly Efficient Solar Steam Generation. *Nano Energy* **2020**, *71* (February), 104650. https://doi.org/10.1016/j.nanoen.2020.104650.

(4) Kim, S. H.; Kang, E. B.; Jeong, C. J.; Sharker, S. M.; In, I.; Park, S. Y. Light Controllable Surface Coating for Effective Photothermal Killing of Bacteria. *ACS Appl. Mater. Interfaces* **2015**, *7* (28), 15600–15606. https://doi.org/10.1021/acsami.5b04321.

(5) Xu, J.-W.; Yao, K.; Xu, Z.-K. Nanomaterials with a Photothermal Effect for Antibacterial Activities: An Overview. *Nanoscale* **2019**, *11* (18), 8680–8691. https://doi.org/10.1039/C9NR01833F.

(6) Yu, H.; Peng, Y.; Yang, Y.; Li, Z. Y. Plasmon-Enhanced Light–Matter Interactions and Applications. *npj Comput. Mater.* **2019**, *5* (1), 1–14. https://doi.org/10.1038/s41524-019-0184-1.

(7) Schuller, J. A.; Barnard, E. S.; Cai, W.; Jun, Y. C.; White, J. S.; Brongersma, M. L. Plasmonics for Extreme Light Concentration and Manipulation. *Nat. Mater.* **2010**, *9* (3), 193–204. https://doi.org/10.1038/nmat2630.

(8) Gärtner, W. W. Photothermal Effect in Semiconductors. *Phys. Rev.* **1961**, *122* (2), 419–424. https://doi.org/10.1103/PhysRev.122.419.

(9) Han, B.; Zhang, Y. L.; Chen, Q. D.; Sun, H. B. Carbon-Based Photothermal Actuators. *Adv. Funct. Mater.* **2018**, *28* (40), 1–23.

https://doi.org/10.1002/adfm.201802235.

(10) Zou, Q.; Abbas, M.; Zhao, L.; Li, S.; Shen, G.; Yan, X. Biological Photothermal Nanodots Based on Self-Assembly of Peptide-Porphyrin Conjugates for Antitumor Therapy. *J. Am. Chem. Soc.* **2017**, *139* (5), 1921–1927. https://doi.org/10.1021/jacs.6b11382.

(11) Wang, J.; Qiu, J. A Review of Organic Nanomaterials in Photothermal Cancer Therapy. *Cancer Res. Front.* **2016**, *2* (1), 67–84. https://doi.org/10.17980/2016.67.

(12) Zheng, X.; Xing, D.; Zhou, F.; Wu, B.; Chen, W. R. Indocyanine Green-Containing Nanostructure as near Infrared Dual-Functional Targeting Probes for Optical Imaging and Photothermal Therapy. *Mol. Pharm.* **2011**, *8* (2), 447–456. https://doi.org/10.1021/mp100301t.

(13) Liu, P. F.; Miao, L.; Deng, Z.; Zhou, J.; Su, H.; Sun, L.; Tanemura, S.; Cao, W.; Jiang, F.; Zhao, L. D. A Mimetic Transpiration System for Record High Conversion Efficiency in Solar Steam Generator under One-Sun. *Mater. Today Energy* **2018**, *8*, 166–173. https://doi.org/10.1016/j.mtener.2018.04.004.

(14) Yue, C.; Liu, P.; Zheng, M.; Zhao, P.; Wang, Y.; Ma, Y.; Cai, L. IR-780 Dye Loaded Tumor Targeting Theranostic Nanoparticles for NIR Imaging and Photothermal Therapy. *Biomaterials* **2013**, *34* (28), 6853–6861. https://doi.org/10.1016/j.biomaterials.2013.05.071.

(15) Landsman, M. L. J.; Kwant, G.; Mook, G. A.; Zijlstra, W. G. Light Absorbing Properties, Stability, and Spectral Stabilization of Indocyanine Green. *J. Appl. Physiol.* **1976**, *40* (4), 575–583. https://doi.org/10.1152/jappl.1976.40.4.575.

(16) Sheng, Z.; Hu, D.; Xue, M.; He, M.; Gong, P.; Cai, L. Indocyanine Green Nanoparticles for Theranostic Applications. *Nano-Micro Lett.* **2013**, *5* (3), 145–150. https://doi.org/10.5101/nml.v5i3.p145-150.

(17) Geng, J.; Sun, C.; Liu, J.; Liao, L. De; Yuan, Y.; Thakor, N.; Wang, J.; Liu, B. Biocompatible Conjugated Polymer Nanoparticles for Efficient Photothermal Tumor Therapy. *Small* **2015**, *11* (13), 1603–1610. https://doi.org/10.1002/smll.201402092.

(18) Song, X.; Chen, Q.; Liu, Z. Recent Advances in the Development of Organic Photothermal Nano-Agents. *Nano Res.* **2015**, *8* (2), 340–354. https://doi.org/10.1007/s12274-014-0620-y.

(19) Yang, K.; Xu, H.; Cheng, L.; Sun, C.; Wang, J.; Liu, Z. In Vitro and in Vivo Near-Infrared Photothermal Therapy of Cancer Using Polypyrrole Organic Nanoparticles. *Adv. Mater.* **2012**, *24* (41), 5586–5592. https://doi.org/10.1002/adma.201202625.

(20) Chen, M.; Fang, X.; Tang, S.; Zheng, N. Polypyrrole Nanoparticles for High-Performance in Vivo near-Infrared Photothermal Cancer Therapy. *Chem. Commun.* **2012**, *48* (71), 8934–8936. https://doi.org/10.1039/c2cc34463g.

(21) Zheng, R.; Wang, S.; Tian, Y.; Jiang, X.; Fu, D.; Shen, S.; Yang, W. Polydopamine-Coated Magnetic Composite Particles with an Enhanced Photothermal Effect. *ACS Appl. Mater. Interfaces* **2015**, *7* (29), 15876–15884. https://doi.org/10.1021/acsami.5b03201.

(22) Farokhi, M.; Mottaghitalab, F.; Saeb, M. R.; Thomas, S. Functionalized Theranostic Nanocarriers with Bio-Inspired Polydopamine for Tumor Imaging and Chemo-Photothermal Therapy. *J. Control. Release* **2019**, *309* (July), 203–219. https://doi.org/10.1016/j.jconrel.2019.07.036.

(23) Liu, Y.; Ai, K.; Lu, L. Polydopamine and Its Derivative Materials: Synthesis and Promising Applications in Energy, Environmental, and Biomedical Fields. *Chem. Rev.* **2014**, *114* (9), 5057–5115. https://doi.org/10.1021/cr400407a.

(24) Zhang, J. Z. Biomedical Applications of Shape-Controlled Plasmonic Nanostructures: A Case Study of Hollow Gold Nanospheres for Photothermal Ablation Therapy of Cancer. *J. Phys. Chem. Lett.* **2010**, *1* (4), 686–695. https://doi.org/10.1021/jz900366c.

(25) Jain, P. K.; Huang, X.; El-Sayed, I. H.; El-Sayed, M. A. Noble Metals on the Nanoscale: Optical and Photothermal Properties and Some Applications in Imaging, Sensing, Biology, and Medicine. *Acc. Chem. Res.* **2008**, *41* (12), 1578–1586. https://doi.org/10.1021/ar7002804.

(26) Coppens, Z. J.; Li, W.; Walker, D. G.; Valentine, J. G. Probing and Controlling

Photothermal Heat Generation in Plasmonic Nanostructures. *Nano Lett.* **2013**, *13* (3), 1023–1028. https://doi.org/10.1021/nl304208s.

(27) Lin, H.; Wang, X.; Yu, L.; Chen, Y.; Shi, J. Two-Dimensional Ultrathin MXene Ceramic Nanosheets for Photothermal Conversion. *Nano Lett.* **2017**, *17* (1), 384–391. https://doi.org/10.1021/acs.nanolett.6b04339.

(28) Yan, H.; Teh, C.; Sreejith, S.; Zhu, L.; Kwok, A.; Fang, W.; Ma, X.; Nguyen, K. T.; Korzh, V.; Zhao, Y. Functional Mesoporous Silica Nanoparticles for Photothermal-Controlled Drug Delivery In Vivo. *Angewandte Chemie*. 2012, pp 8498–8502. https://doi.org/10.1002/ange.201203993.

(29) Liu, H.; Chen, D.; Li, L.; Liu, T.; Tan, L.; Wu, X.; Tang, F. Multifunctional Gold Nanoshells on Silica Nanorattles: A Platform for the Combination of Photothermal Therapy and Chemotherapy with Low Systemic Toxicity. *Angew. Chemie* **2011**, *123* (4), 921–925. https://doi.org/10.1002/ange.201002820.

(30) Sun, Z.; Xie, H.; Tang, S.; Yu, X. F.; Guo, Z.; Shao, J.; Zhang, H.; Huang, H.; Wang, H.; Chu, P. K. Ultrasmall Black Phosphorus Quantum Dots: Synthesis and Use as Photothermal Agents. *Angew. Chemie - Int. Ed.* **2015**, *54* (39), 11526–11530. https://doi.org/10.1002/anie.201506154.

(31) Yong, Y.; Cheng, X.; Bao, T.; Zu, M.; Yan, L.; Yin, W.; Ge, C.; Wang, D.; Gu, Z.; Zhao, Y. Tungsten Sulfide Quantum Dots as Multifunctional Nanotheranostics for in Vivo Dual-Modal Image-Guided Photothermal/Radiotherapy Synergistic Therapy. *ACS Nano* **2015**, *9* (12), 12451–12463. https://doi.org/10.1021/acsnano.5b05825.

(32) Huang, H. C.; Barua, S.; Sharma, G.; Dey, S. K.; Rege, K. Inorganic Nanoparticles for Cancer Imaging and Therapy. *J. Control. Release* **2011**, *155* (3), 344–357. https://doi.org/10.1016/j.jconrel.2011.06.004.

(33) Jain, P. K.; El-Sayed, I. H.; El-Sayed, M. A. Au Nanoparticles Target Cancer. *Nano Today* **2007**, *2* (1), 18–29. https://doi.org/10.1016/S1748-0132(07)70016-6.

(34) Huang, X.; El-Sayed, I. H.; Qian, W.; El-Sayed, M. A. Cancer Cell Imaging and Photothermal Therapy in the Near-Infrared Region by Using Gold Nanorods. *J. Am. Chem. Soc.* **2006**, *128* (6), 2115–2120. https://doi.org/10.1021/ja057254a.

(35) Ali, M. R. K.; Rahman, M. A.; Wu, Y.; Han, T.; Peng, X.; Mackey, M. A.; Wang, D.; Shin, H. J.; Chen, Z. G.; Xiao, H.; Wu, R.; Tang, Y.; Shin, D. M.; El-Sayed, M. A. Efficacy, Long-Term Toxicity, and Mechanistic Studies of Gold Nanorods Photothermal Therapy of Cancer in Xenograft Mice. *Proc. Natl. Acad. Sci. U. S. A.* **2017**, *114* (15), E3110–E3118. https://doi.org/10.1073/pnas.1619302114.

(36) Dickerson, E. B.; Dreaden, E. C.; Huang, X.; El-Sayed, I. H.; Chu, H.; Pushpanketh, S.; McDonald, J. F.; El-Sayed, M. A. Gold Nanorod Assisted Near-Infrared Plasmonic Photothermal Therapy (PPTT) of Squamous Cell Carcinoma in Mice. *Cancer Lett.* **2008**, *269* (1), 57–66. https://doi.org/10.1016/j.canlet.2008.04.026.

(37) Choi, W. Il; Kim, J. Y.; Kang, C.; Byeon, C. C.; Kim, Y. H.; Tae, G. Tumor Regression in Vivo by Photothermal Therapy Based on Gold-Nanorod-Loaded, Functional Nanocarriers. *ACS Nano* **2011**, *5* (3), 1995–2003. https://doi.org/10.1021/nn103047r.

(38) Chen, J.; Glaus, C.; Laforest, R.; Zhang, Q.; Yang, M.; Gidding, M.; Welch, M. J.; Xia, Y. Gold Nanocages as Photothermal Transducers for Cancer Treatment. *Small* **2010**, *6* (7), 811–817. https://doi.org/10.1002/smll.200902216.

(39) Skrabalak, S. E.; Chen, J.; Au, L.; Lu, X.; Li, X.; Xia, Y. Gold Nanocages for Biomedical Applications. *Adv. Mater.* **2007**, *19* (20), 3177–3184. https://doi.org/10.1002/adma.200701972.

(40) El-Sayed, I. H.; Huang, X.; El-Sayed, M. A. Selective Laser Photo-Thermal Therapy of Epithelial Carcinoma Using Anti-EGFR Antibody Conjugated Gold Nanoparticles. *Cancer Lett.* **2006**, *239* (1), 129–135. https://doi.org/10.1016/j.canlet.2005.07.035.

(41) Piao, J. G.; Wang, L.; Gao, F.; You, Y. Z.; Xiong, Y.; Yang, L. Erythrocyte Membrane Is an Alternative Coating to Polyethylene Glycol for Prolonging the Circulation Lifetime of Gold Nanocages for Photothermal Therapy. *ACS Nano* **2014**, *8* (10), 10414–10425. https://doi.org/10.1021/nn503779d.

(42) Ma, Y.; Liang, X.; Tong, S.; Bao, G.; Ren, Q.; Dai, Z. Gold Nanoshell

Nanomicelles for Potential Magnetic Resonance Imaging, Light-Triggered Drug Release, and Photothermal Therapy. *Adv. Funct. Mater.* **2013**, *23* (7), 815–822. https://doi.org/10.1002/adfm.201201663.

(43) Melancon, M. P.; Elliott, A.; Ji, X.; Shetty, A.; Yang, Z.; Tian, M.; Taylor, B.; Stafford, R. J.; Li, C. Theranostics with Multifunctional Magnetic Gold Nanoshells: Photothermal Therapy and T2* Magnetic Resonance Imaging. *Invest. Radiol.* **2011**, *46* (2), 132–140. https://doi.org/10.1097/RLI.0b013e3181f8e7d8.

(44) Liu, H.; Chen, D.; Li, L.; Liu, T.; Tan, L.; Wu, X.; Tang, F. Multifunctional Gold Nanoshells on Silica Nanorattles: A Platform for the Combination of Photothermal Therapy and Chemotherapy with Low Systemic Toxicity. *Angew. Chemie - Int. Ed.* **2011**, *50* (4), 891–895. https://doi.org/10.1002/anie.201002820.

(45) Kim, J.; Park, S.; Lee, J. E.; Jin, S. M.; Lee, J. H.; Lee, I. S.; Yang, I.; Kim, J.-S.; Kim, S. K.; Cho, M.-H.; Hyeon, T. Designed Fabrication of Multifunctional Magnetic Gold Nanoshells and Their Application to Magnetic Resonance Imaging and Photothermal Therapy. *Angew. Chemie* **2006**, *118* (46), 7918–7922. https://doi.org/10.1002/ange.200602471.

(46) Hu, M.; Chen, J.; Li, Z. Y.; Au, L.; Hartland, G. V.; Li, X.; Marquez, M.; Xia, Y. Gold Nanostructures: Engineering Their Plasmonic Properties for Biomedical Applications. *Chem. Soc. Rev.* **2006**, *35* (11), 1084–1094. https://doi.org/10.1039/b517615h.

(47) Mayer, K. M.; Hafner, J. H. Localized Surface Plasmon Resonance Sensors. *Chem. Rev.* **2011**, *111* (6), 3828–3857. https://doi.org/10.1021/cr100313v.

(48) Huang, X.; Jain, P. K.; El-Sayed, I. H.; El-Sayed, M. A. Plasmonic Photothermal Therapy (PPTT) Using Gold Nanoparticles. *Lasers Med. Sci.* **2008**, *23* (3), 217–228. https://doi.org/10.1007/s10103-007-0470-x.

(49) Nikoobakht, B.; El-Sayed, M. A. Preparation and Growth Mechanism of Gold Nanorods (NRs) Using Seed-Mediated Growth Method. *Chem. Mater.* **2003**, *15* (10), 1957–1962. https://doi.org/10.1021/cm020732l.

(50) Yavuz, M. S.; Cheng, Y.; Chen, J.; Cobley, C. M.; Zhang, Q.; Rycenga, M.; Xie,

J.; Kim, C.; Song, K. H.; Schwartz, A. G.; Wang, L. V.; Xia, Y. Gold Nanocages Covered by Smart Polymers for Controlled Release with Near-Infrared Light. *Nat. Mater.* **2009**, *8* (12), 935–939. https://doi.org/10.1038/nmat2564.

(51) Riley, R. S.; Day, E. S. Gold Nanoparticle-Mediated Photothermal Therapy: Applications and Opportunities for Multimodal Cancer Treatment. *Wiley Interdiscip. Rev. Nanomedicine Nanobiotechnology* **2017**, *9* (4). https://doi.org/10.1002/wnan.1449.

(52) Becker, A.; Hessenius, C.; Licha, K.; Ebert, B.; Sukowski, U.; Semmler, W.; Wiedenmann, B.; Grötzinger, C. Receptor-Targeted Optical Imaging of Tumors with near-Infrared Fluorescent Ligands. *Nat. Biotechnol.* **2001**, *19* (4), 327–331. https://doi.org/10.1038/86707.

(53) Riley, R. S.; Day, E. S. Gold Nanoparticle-Mediated Photothermal Therapy: Applications and Opportunities for Multimodal Cancer Treatment. *Wiley Interdiscip. Rev. Nanomedicine Nanobiotechnology* **2017**, *9* (4). https://doi.org/10.1002/wnan.1449.

(54) Chen, J.; Wang, D.; Xi, J.; Au, L.; Siekkinen, A.; Warsen, A.; Li, Z. Y.; Zhang, H.; Xia, Y.; Li, X. Immuno Gold Nanocages with Tailored Optical Properties for Targeted Photothermal Destruction of Cancer Cells. *Nano Lett.* **2007**, *7* (5), 1318–1322. https://doi.org/10.1021/nl070345g.

(55) Huang, X.; Qian, W.; El-Sayed, I. H.; El-Sayed, M. A. The Potential Use of the Enhanced Nonlinear Properties of Gold Nanospheres in Photothermal Cancer Therapy. *Lasers Surg. Med.* **2007**, *39* (9), 747–753. https://doi.org/10.1002/lsm.20577.

(56) Murphy, C. J.; Gole, A. M.; Stone, J. W.; Sisco, P. N.; Alkilany, A. M.; Goldsmith, E. C.; Baxter, S. C. Gold Nanoparticles in Biology: Beyond Toxicity to Cellular Imaging. *Acc. Chem. Res.* **2008**, *41* (12), 1721–1730. https://doi.org/10.1021/ar800035u.

(57) Huang, X.; Jain, P. K.; El-Sayed, I. H.; El-Sayed, M. A. Gold Nanoparticles: Interesting Optical Properties and Recent Applications in Cancer Diagnostics and Therapy. *Nanomedicine* **2007**, *2* (5), 681–693.

https://doi.org/10.2217/17435889.2.5.681.

(58) Singh, P.; Pandit, S.; Mokkapati, V. R. S. S.; Garg, A.; Ravikumar, V.; Mijakovic, I. Gold Nanoparticles in Diagnostics and Therapeutics for Human Cancer. *Int. J. Mol. Sci.* **2018**, *19* (7). https://doi.org/10.3390/ijms19071979.

(59) Silica-Coated Gold−Silver Nanocages as Photothermal Antibacterial.Pdf.

(60) Hu, B.; Wang, N.; Han, L.; Chen, M. L.; Wang, J. H. Core-Shell-Shell Nanorods for Controlled Release of Silver That Can Serve as a Nanoheater for Photothermal Treatment on Bacteria. *Acta Biomater.* **2015**, *11* (1), 511–519. https://doi.org/10.1016/j.actbio.2014.09.005.

(61) Grisoli, P.; De Vita, L.; Milanese, C.; Taglietti, A.; Fernandez, Y. D.; Bouzin, M.; D'alfonso, L.; Sironi, L.; Rossi, S.; Vigani, B.; Sperandeo, P.; Polissi, A.; Pallavicini, P. Pva Films with Mixed Silver Nanoparticles and Gold Nanostars for Intrinsic and Photothermal Antibacterial Action. *Nanomaterials* **2021**, *11* (6). https://doi.org/10.3390/nano11061387.

(62) Ong, C.; Lim, J. Z. Z.; Ng, C.-T.; Li, J. J.; Yung, L.-Y. L.; Bay, B.-H. Silver Nanoparticles in Cancer: Therapeutic Efficacy and Toxicity. *Curr. Med. Chem.* **2013**, *20* (6), 772–781. https://doi.org/10.2174/0929867311320060003.

(63) Austin, L. A.; MacKey, M. A.; Dreaden, E. C.; El-Sayed, M. A. The Optical, Photothermal, and Facile Surface Chemical Properties of Gold and Silver Nanoparticles in Biodiagnostics, Therapy, and Drug Delivery. *Arch. Toxicol.* **2014**, *88* (7), 1391–1417. https://doi.org/10.1007/s00204-014-1245-3.

(64) Wei, L.; Lu, J.; Xu, H.; Patel, A.; Chen, Z. S.; Chen, G. Silver Nanoparticles: Synthesis, Properties, and Therapeutic Applications. *Drug Discov. Today* **2015**, *20* (5), 595–601. https://doi.org/10.1016/j.drudis.2014.11.014.

(65) Bi, X.; Bai, Q.; Liang, M.; Yang, D.; Li, S.; Wang, L.; Liu, J.; Yu, W. W.; Sui, N.; Zhu, Z. Silver Peroxide Nanoparticles for Combined Antibacterial Sonodynamic and Photothermal Therapy. **2022**, *2104160*, 1–11. https://doi.org/10.1002/smll.202104160.

(66) Nakal-Chidiac, A.; García, O.; García-Fernández, L.; Martín-Saavedra, F. M.;

Sánchez-Casanova, S.; Escudero-Duch, C.; San Román, J.; Vilaboa, N.; Aguilar, M. R. Chitosan-Stabilized Silver Nanoclusters with Luminescent, Photothermal and Antibacterial Properties. *Carbohydr. Polym.* **2020**, *250* (May). https://doi.org/10.1016/j.carbpol.2020.116973.

(67) Tee, S. I. Y. I. N.; Win, Y. I. N.; Goh, S. S. *Introduction to Photothermal Nanomaterials*; 2022.

(68) Balandin, A. A. Thermal Properties of Graphene and Nanostructured Carbon Materials. *Nat. Mater.* **2011**, *10* (8), 569–581. https://doi.org/10.1038/nmat3064.

(69) Hu, X.; Xu, W.; Zhou, L.; Tan, Y.; Wang, Y.; Zhu, S.; Zhu, J. Tailoring Graphene Oxide-Based Aerogels for Efficient Solar Steam Generation under One Sun. *Advanced Materials*. 2017. https://doi.org/10.1002/adma.201604031.

(70) Jiang, F.; Liu, H.; Li, Y.; Kuang, Y.; Xu, X.; Chen, C.; Huang, H.; Jia, C.; Zhao, X.; Hitz, E.; Zhou, Y.; Yang, R.; Cui, L.; Hu, L. Lightweight, Mesoporous, and Highly Absorptive All-Nanofiber Aerogel for Efficient Solar Steam Generation. *ACS Appl. Mater. Interfaces* **2018**, *10* (1), 1104–1112. https://doi.org/10.1021/acsami.7b15125.

(71) Chen, C.; Li, Y.; Song, J.; Yang, Z.; Kuang, Y.; Hitz, E.; Jia, C.; Gong, A.; Jiang, F.; Zhu, J. Y.; Yang, B.; Xie, J.; Hu, L. Highly Flexible and Efficient Solar Steam Generation Device. *Adv. Mater.* **2017**, *29* (30), 1–8. https://doi.org/10.1002/adma.201701756.

(72) Yang, J.; Pang, Y.; Huang, W.; Shaw, S. K.; Schiffbauer, J.; Pillers, M. A.; Mu, X.; Luo, S.; Zhang, T.; Huang, Y.; Li, G.; Ptasinska, S.; Lieberman, M.; Luo, T. Functionalized Graphene Enables Highly Efficient Solar Thermal Steam Generation. *ACS Nano* **2017**, *11* (6), 5510–5518. https://doi.org/10.1021/acsnano.7b00367.

(73) Liu, K. K.; Jiang, Q.; Tadepalli, S.; Raliya, R.; Biswas, P.; Naik, R. R.; Singamaneni, S. Wood-Graphene Oxide Composite for Highly Efficient Solar Steam Generation and Desalination. *ACS Appl. Mater. Interfaces* **2017**, *9* (8), 7675–7681. https://doi.org/10.1021/acsami.7b01307.

(74) Wang, G.; Fu, Y.; Ma, X.; Pi, W.; Liu, D.; Wang, X. Reusable Reduced

Graphene Oxide Based Double-Layer System Modified by Polyethylenimine for Solar Steam Generation. *Carbon N. Y.* **2017**, *114*, 117–124. https://doi.org/10.1016/j.carbon.2016.11.071.

(75) Yin, Z.; Wang, H.; Jian, M.; Li, Y.; Xia, K.; Zhang, M.; Wang, C.; Wang, Q.; Ma, M.; Zheng, Q. S.; Zhang, Y. Extremely Black Vertically Aligned Carbon Nanotube Arrays for Solar Steam Generation. *ACS Appl. Mater. Interfaces* **2017**, *9* (34), 28596–28603. https://doi.org/10.1021/acsami.7b08619.

(76) Kuzmenko, A. B.; Van Heumen, E.; Carbone, F.; Van Der Marel, D. Universal Optical Conductance of Graphite. *Phys. Rev. Lett.* **2008**, *100* (11), 2–5. https://doi.org/10.1103/PhysRevLett.100.117401.

(77) Deng, Z.; Zhou, J.; Miao, L.; Liu, C.; Peng, Y.; Sun, L.; Tanemura, S. The Emergence of Solar Thermal Utilization: Solar-Driven Steam Generation. *J. Mater. Chem. A* **2017**, *5* (17), 7691–7709. https://doi.org/10.1039/c7ta01361b.

(78) Shi, L.; Wang, Y.; Zhang, L.; Wang, P. Rational Design of a Bi-Layered Reduced Graphene Oxide Film on Polystyrene Foam for Solar-Driven Interfacial Water Evaporation. *J. Mater. Chem. A* **2017**, *5* (31), 16212–16219. https://doi.org/10.1039/c6ta09810j.

(79) Jia, C.; Li, Y.; Yang, Z.; Chen, G.; Yao, Y.; Jiang, F.; Kuang, Y.; Pastel, G.; Xie, H.; Yang, B.; Das, S.; Hu, L. Rich Mesostructures Derived from Natural Woods for Solar Steam Generation. *Joule* **2017**, *1* (3), 588–599. https://doi.org/10.1016/j.joule.2017.09.011.

(80) Dao, V.-D.; Choi, H.-S. Carbon-Based Sunlight Absorbers in Solar-Driven Steam Generation Devices. *Global Challenges*. 2018, p 1700094. https://doi.org/10.1002/gch2.201700094.

(81) Xu, N.; Hu, X.; Xu, W.; Li, X.; Zhou, L.; Zhu, S.; Zhu, J. Mushrooms as Efficient Solar Steam-Generation Devices. *Advanced Materials*. 2017. https://doi.org/10.1002/adma.201606762.

(82) Zhang, Q.; Xu, W.; Wang, X. Carbon Nanocomposites with High Photothermal Conversion Efficiency. *Sci. China Mater.* **2018**, *61* (7), 905–914. https://doi.org/10.1007/s40843-018-9250-x.

(83) Biju, V. Chemical Modifications and Bioconjugate Reactions of Nanomaterials for Sensing, Imaging, Drug Delivery and Therapy. *Chem. Soc. Rev.* **2014**, *43* (3), 744–764. https://doi.org/10.1039/c3cs60273g.

(84) Chen, J.; Ning, C.; Zhou, Z.; Yu, P.; Zhu, Y.; Tan, G.; Mao, C. Nanomaterials as Photothermal Therapeutic Agents. *Prog. Mater. Sci.* **2019**, *99* (May 2017), 1–26. https://doi.org/10.1016/j.pmatsci.2018.07.005.

(85) Kaur, J.; Gill, G. S.; Jeet, K. *Applications of Carbon Nanotubes in Drug Delivery: A Comprehensive Review. A Comprehensive Review.*; Elsevier Inc., 2018. https://doi.org/10.1016/B978-0-12-814031-4.00005-2.

(86) Burlaka, O. M.; Pirko, Y. V.; Yemets, A. I.; Blume, Y. B. Plant Genetic Transformation Using Carbon Nanotubes for DNA Delivery. *Cytol. Genet.* **2015**, *49* (6), 349–357. https://doi.org/10.3103/S009545271506002X.

(87) Tan, L.; Li, J.; Liu, X.; Cui, Z.; Yang, X.; Zhu, S.; Li, Z.; Yuan, X.; Zheng, Y.; Yeung, K. W. K.; Pan, H.; Wang, X.; Wu, S. Rapid Biofilm Eradication on Bone Implants Using Red Phosphorus and Near-Infrared Light. *Adv. Mater.* **2018**, *30* (31), 1–10. https://doi.org/10.1002/adma.201801808.

(88) Bruellhoff, K.; Fiedler, J.; Möller, M.; Groll, J.; Brenner, R. E. Surface Coating Strategies to Prevent Biofilm Formation on Implant Surfaces. *Int. J. Artif. Organs* **2010**, *33* (9), 646–653. https://doi.org/10.1177/039139881003300910.

(89) Wang, C.; Zhao, W.; Cao, B.; Wang, Z.; Zhou, Q.; Lu, S.; Lu, L.; Zhan, M. Bio Fi Lm-Responsive Polymeric Nanoparticles with Self-Adaptive Deep Penetration for In Vivo Photothermal Treatment of Implant Infection. **2020**. https://doi.org/10.1021/acs.chemmater.0c02055.

(90) Hu, D.; Li, H.; Wang, B.; Ye, Z.; Lei, W.; Jia, F.; Jin, Q.; Ren, K. F.; Ji, J. Surface-Adaptive Gold Nanoparticles with Effective Adherence and Enhanced Photothermal Ablation of Methicillin-Resistant Staphylococcus Aureus Biofilm. *ACS Nano* **2017**, *11* (9), 9330–9339. https://doi.org/10.1021/acsnano.7b04731.

(91) Pallavicini, P.; Dona, A.; Taglietti, A.; Minzioni, P.; Patrini, M.; Dacarro, G.; Chirico, G.; Sironi, L.; Bloise, N.; Visaie, L.; Scarabelli, L. Self-Assembled Monolayers of Gold Nanostars: A Convenient Tool for near-IR Photothermal

Biofilm Eradication. *Chem. Commun.* **2014**, *50* (16), 1969–1971. https://doi.org/10.1039/c3cc48667b.

(92) Yuan, Z.; Tao, B.; He, Y.; Liu, J.; Lin, C.; Shen, X.; Ding, Y.; Yu, Y.; Mu, C.; Liu, P.; Cai, K. Biocompatible MoS2/PDA-RGD Coating on Titanium Implant with Antibacterial Property via Intrinsic ROS-Independent Oxidative Stress and NIR Irradiation. *Biomaterials* **2019**, *217* (March). https://doi.org/10.1016/j.biomaterials.2019.119290.

(93) Lei, W.; Ren, K.; Chen, T.; Chen, X.; Li, B.; Chang, H.; Ji, J. Polydopamine Nanocoating for Effective Photothermal Killing of Bacteria and Fungus upon Near-Infrared Irradiation. *Advanced Materials Interfaces*. 2016. https://doi.org/10.1002/admi.201600767.

(94) Wang, Z.; Yan, Y.; Shen, X.; Jin, C.; Sun, Q.; Li, H. A Wood-Polypyrrole Composite as a Photothermal Conversion Device for Solar Evaporation Enhancement. *J. Mater. Chem. A* **2019**, *7* (36), 20706–20712. https://doi.org/10.1039/c9ta04914b.

(95) Tao, F.; Zhang, Y.; Yin, K.; Cao, S.; Chang, X.; Lei, Y.; Wang, D. S.; Fan, R.; Dong, L.; Yin, Y.; Chen, X. Copper Sulfide-Based Plasmonic Photothermal Membrane for High-Efficiency Solar Vapor Generation. *ACS Appl. Mater. Interfaces* **2018**, *10* (41), 35154–35163. https://doi.org/10.1021/acsami.8b11786.

(96) Shao, B.; Wu, X.; Wang, Y.; Gao, T.; Liu, Z.-Q.; Owens, G.; Xu, H. A General Method for Selectively Coating Photothermal Materials on 3D Porous Substrate Surfaces towards Cost-Effective and Highly Efficient Solar Steam Generation. *J. Mater. Chem. A* **2020**, *8* (46), 24703–24709. https://doi.org/10.1039/D0TA08539A.

(97) Kurapati, R.; Vaidyanathan, M.; Raichur, A. M. Synergistic Photothermal Antimicrobial Therapy Using Graphene Oxide/Polymer Composite Layer-by-Layer Thin Films. *RSC Adv.* **2016**, *6* (46), 39852–39860. https://doi.org/10.1039/c5ra23038a.

(98) Jaque, D.; Mar Inez Maestro, L.; Del Rosal, B.; Haro-Gonzalez, P.; Benayas, A.; Plaza, J. L.; Mar, E.; Iguez, R.; Gar, J.; Soí, I. Nanoparticles for Photothermal

Therapies. https://doi.org/10.1039/c4nr00708e.

(99) Vines, J. B.; Yoon, J. H.; Ryu, N. E.; Lim, D. J.; Park, H. Gold Nanoparticles for Photothermal Cancer Therapy. *Front. Chem.* **2019**, *7* (APR), 1–16. https://doi.org/10.3389/fchem.2019.00167.

(100) Zou, Y.; Zhang, Y.; Yu, Q.; Chen, H. Photothermal Bactericidal Surfaces: Killing Bacteria Using Light Instead of Biocides. *Biomater. Sci.* **2021**, *9* (1), 10–22. https://doi.org/10.1039/D0BM00617C.

(101) Wang, P. Emerging Investigator Series: The Rise of Nano-Enabled Photothermal Materials for Water Evaporation and Clean Water Production by Sunlight. *Environ. Sci. Nano* **2018**, *5* (5), 1078–1089. https://doi.org/10.1039/C8EN00156A.

(102) Du, W.; Jin, Y.; Shi, L.; Shen, Y.; Lai, S.; Zhou, Y. NIR-Light-Induced Thermoset Shape Memory Polyurethane Composites with Self-Healing and Recyclable Functionalities. *Compos. Part B Eng.* **2020**, *195*, 108092. https://doi.org/10.1016/J.COMPOSITESB.2020.108092.

(103) Zhang, X.; Tan, B.; Wu, Y.; Zhang, M.; Liao, J. A Review on Hydrogels with Photothermal Effect in Wound Healing and Bone Tissue Engineering. *Polymers (Basel).* **2021**, *13* (13), 2100. https://doi.org/10.3390/polym13132100.

(104) De Sio, L.; Ding, B.; Focsan, M.; Kogermann, K.; Pascoal- Faria, P.; Petronela, F.; Mitchell, G.; Zussman, E.; Pierini, F. Personalized Reusable Face Masks with Smart Nano- Assisted Destruction of Pathogens for COVID- 19: A Visionary Road. *Chem. – A Eur. J.* **2021**, *27* (20), 6112–6130. https://doi.org/10.1002/chem.202004875.

(105) Wang, J.; Li, Y.; Deng, L.; Wei, N.; Weng, Y.; Dong, S.; Qi, D.; Qiu, J.; Chen, X.; Wu, T. High-Performance Photothermal Conversion of Narrow-Bandgap Ti 2 O 3 Nanoparticles. https://doi.org/10.1002/adma.201603730.

(106) Norouzi, H.; Khoshgard, K.; Akbarzadeh, F. In Vitro Outlook of Gold Nanoparticles in Photo-Thermal Therapy: A Literature Review. *Lasers Med. Sci.* **2018**, *33* (4), 917–926. https://doi.org/10.1007/s10103-018-2467-z.

(107) Estelrich, J.; Busquets, M. Iron Oxide Nanoparticles in Photothermal Therapy. *Molecules* **2018**, *23* (7), 1567. https://doi.org/10.3390/molecules23071567.

(108) Kim, M.; Lee, J.; Nam, J. Plasmonic Photothermal Nanoparticles for Biomedical Applications. *Adv. Sci.* **2019**, *6* (17), 1900471. https://doi.org/10.1002/advs.201900471.

(109) Liu, Y.; Li, F.; Guo, Z.; Xiao, Y.; Zhang, Y.; Sun, X.; Zhe, T.; Cao, Y.; Wang, L.; Lu, Q.; Wang, J. Silver Nanoparticle-Embedded Hydrogel as a Photothermal Platform for Combating Bacterial Infections. *Chem. Eng. J.* **2020**, *382*, 122990. https://doi.org/10.1016/J.CEJ.2019.122990.

(110) Wijenayaka, L. A.; Wijesena, R. N.; Tissera, N. D.; Bandara, W. R. L. N.; Amaratunga, G. J.; Silva, K. M. N. De. Infrared Absorbing Nanoparticle Impregnated Self-Heating Fabrics for Significantly Improved Moisture Management under Ambient Conditions. *R. Soc. Open Sci.* **2021**. https://doi.org/10.1098/RSOS.202222.

(111) Li, Z.; Lei, H.; Kan, A.; Xie, H.; Yu, W. Photothermal Applications Based on Graphene and Its Derivatives: A State-of-the-Art Review. *Energy* **2021**, *216*, 119262. https://doi.org/10.1016/J.ENERGY.2020.119262.

(112) Sobhani, Z.; Behnam, M. A.; Emami, F.; Dehghanian, A.; Jamhiri, I. Photothermal Therapy of Melanoma Tumor Using Multiwalled Carbon Nanotubes. *Int. J. Nanomedicine* **2017**, *12*, 4509–4517. https://doi.org/10.2147/IJN.S134661.

(113) Geng, B.; Yang, D.; Pan, D.; Wang, L.; Zheng, F.; Shen, W.; Zhang, C.; Li, X. NIR-Responsive Carbon Dots for Efficient Photothermal Cancer Therapy at Low Power Densities. *Carbon N. Y.* **2018**, *134*, 153–162. https://doi.org/10.1016/J.CARBON.2018.03.084.

(114) Oruc, B.; Unal, H. Fluorophore-Decorated Carbon Nanotubes with Enhanced Photothermal Activity as Antimicrobial Nanomaterials. *ACS Omega* **2019**, *4* (3), 5556–5564. https://doi.org/10.1021/acsomega.9b00099.

(115) Jung, H. S.; Verwilst, P.; Sharma, A.; Shin, J.; Sessler, J. L.; Kim, J. S. Organic Molecule-Based Photothermal Agents: An Expanding Photothermal Therapy

Universe. *Chem. Soc. Rev.* **2018**, *47* (7), 2280–2297. https://doi.org/10.1039/C7CS00522A.

(116) Bilici, K.; Atac, N.; Muti, A.; Baylam, I.; Dogan, O.; Sennaroglu, A.; Can, F.; Yagci Acar, H. Broad Spectrum Antibacterial Photodynamic and Photothermal Therapy Achieved with Indocyanine Green Loaded SPIONs under near Infrared Irradiation. *Biomater. Sci.* **2020**, *8* (16), 4616–4625. https://doi.org/10.1039/D0BM00821D.

(117) Xu, L.; Cheng, L.; Wang, C.; Peng, R.; Liu, Z. Conjugated Polymers for Photothermal Therapy of Cancer. *Polym. Chem.* **2014**, *5* (5), 1573–1580. https://doi.org/10.1039/C3PY01196H.

(118) Lin, F.; Duan, Q.-Y.; Wu, F.-G. Conjugated Polymer-Based Photothermal Therapy for Killing Microorganisms. *ACS Appl. Polym. Mater.* **2020**, *2* (10), 4331–4344. https://doi.org/10.1021/acsapm.0c00718.

(119) Lee, H.; Dellatore, S. M.; Miller, W. M.; Messersmith, P. B. Mussel-Inspired Surface Chemistry for Multifunctional Coatings. *Science (80-.).* **2007**, *318* (5849), 426–430. https://doi.org/10.1126/science.1147241.

(120) Zheng, R.; Wang, S.; Tian, Y.; Jiang, X.; Fu, D.; Shen, S.; Yang, W. Polydopamine-Coated Magnetic Composite Particles with an Enhanced Photothermal Effect. *ACS Appl. Mater. Interfaces* **2015**, *7* (29), 15876–15884. https://doi.org/10.1021/acsami.5b03201.

(121) Wang, C.; Bai, J.; Liu, Y.; Jia, X.; Jiang, X. Polydopamine Coated Selenide Molybdenum: A New Photothermal Nanocarrier for Highly Effective Chemo-Photothermal Synergistic Therapy. *ACS Biomater. Sci. Eng.* **2016**, *2* (11), 2011–2017. https://doi.org/10.1021/acsbiomaterials.6b00416.

(122) Ding, F.; Gao, X.; Huang, X.; Ge, H.; Xie, M.; Qian, J.; Song, J.; Li, Y.; Zhu, X.; Zhang, C. Polydopamine-Coated Nucleic Acid Nanogel for SiRNA-Mediated Low-Temperature Photothermal Therapy. *Biomaterials* **2020**, *245*, 119976. https://doi.org/10.1016/J.BIOMATERIALS.2020.119976.

(123) Tas, C. E.; Berksun, E.; Koken, D.; Unal, S.; Unal, H. Photothermal Waterborne Polydopamine/Polyurethanes with Light-to-Heat Conversion Properties. *ACS*

Appl. Polym. Mater. **2021**, *3* (8), 3929–3940. https://doi.org/10.1021/acsapm.1c00495.

(124) Shvedova, A. A.; Kagan, V. E.; Fadeel, B. Close Encounters of the Small Kind: Adverse Effects of Man-Made Materials Interfacing with the Nano-Cosmos of Biological Systems. *Annu. Rev. Pharmacol. Toxicol.* **2010**, *50*, 63–88. https://doi.org/10.1146/annurev.pharmtox.010909.105819.

(125) Fadeel, B. Hide and Seek: Nanomaterial Interactions With the Immune System. *Front. Immunol.* **2019**, *10*, 133. https://doi.org/10.3389/fimmu.2019.00133.

(126) Satish, S.; Tharmavaram, M.; Rawtani, D. Halloysite Nanotubes as a Nature's Boon for Biomedical Applications. *Nanobiomedicine* **2019**, *6*, 1849543519863625. https://doi.org/10.1177/1849543519863625.

(127) Luo, X.; Zhang, J.; Wu, Y.-P.; Yang, X.; Kuang, X.-P.; Li, W.-X.; Li, Y.-F.; He, R.-R.; Liu, M. Multifunctional HNT@Fe_3O_4@PPy@DOX Nanoplatform for Effective Chemo-Photothermal Combination Therapy of Breast Cancer with MR Imaging. *ACS Biomater. Sci. Eng.* **2020**, *6* (6), 3361–3374. https://doi.org/10.1021/acsbiomaterials.9b01709.

(128) Wang, B.; Han, Z.; Song, B.; Yu, L.; Ma, Z.; Xu, H.; Qiao, M. Effective Drug Delivery System Based on Hydrophobin and Halloysite Clay Nanotubes for Sustained Release of Doxorubicin. *Colloids Surfaces A Physicochem. Eng. Asp.* **2021**, *628*, 127351. https://doi.org/10.1016/J.COLSURFA.2021.127351.

(129) De Silva, R. T.; Dissanayake, R. K.; Mantilaka, M. M. M. G. P. G.; Wijesinghe, W. P. S. L.; Kaleel, S. S.; Premachandra, T. N.; Weerasinghe, L.; Amaratunga, G. A. J.; de Silva, K. M. N. Drug-Loaded Halloysite Nanotube-Reinforced Electrospun Alginate-Based Nanofibrous Scaffolds with Sustained Antimicrobial Protection. *ACS Appl. Mater. Interfaces* **2018**, *10* (40), 33913–33922. https://doi.org/10.1021/acsami.8b11013.

(130) Zahidah, K. A.; Kakooei, S.; Ismail, M. C.; Bothi Raja, P. Halloysite Nanotubes as Nanocontainer for Smart Coating Application: A Review. *Prog. Org. Coatings* **2017**, *111* (May), 175–185. https://doi.org/10.1016/j.porgcoat.2017.05.018.

(131) Hendessi, S.; Sevinis, E. B.; Unal, S.; Cebeci, F. C.; Menceloglu, Y. Z.; Unal, H. Antibacterial Sustained-Release Coatings from Halloysite Nanotubes/Waterborne Polyurethanes. *Progress in Organic Coatings*. 2016, pp 253–261. https://doi.org/10.1016/j.porgcoat.2016.09.005.

(132) Alkan Tas, B.; Sehit, E.; Erdinc Tas, C.; Unal, S.; Cebeci, F. C.; Menceloglu, Y. Z.; Unal, H. Carvacrol Loaded Halloysite Coatings for Antimicrobial Food Packaging Applications. *Food Packag. Shelf Life* **2019**, *20*, 100300. https://doi.org/10.1016/J.FPSL.2019.01.004.

(133) Goda, E. S.; Gab-Allah, M. A.; Singu, B. S.; Yoon, K. R. Halloysite Nanotubes Based Electrochemical Sensors: A Review. *Microchem. J.* **2019**, *147*, 1083–1096. https://doi.org/10.1016/J.MICROC.2019.04.011.

(134) Goda, E. S.; Yoon, K. R.; El-sayed, S. H.; Hong, S. E. Halloysite Nanotubes as Smart Flame Retardant and Economic Reinforcing Materials: A Review. *Thermochim. Acta* **2018**, *669*, 173–184. https://doi.org/10.1016/J.TCA.2018.09.017.

(135) Li, Q.; Ren, T.; Perkins, P.; Hu, X.; Wang, X. Applications of Halloysite Nanotubes in Food Packaging for Improving Film Performance and Food Preservation. *Food Control* **2021**, *124*, 107876. https://doi.org/10.1016/J.FOODCONT.2021.107876.

(136) Tas, C. E.; Hendessi, S.; Baysal, M.; Unal, S.; Cebeci, F. C.; Menceloglu, Y. Z.; Unal, H. Halloysite Nanotubes/Polyethylene Nanocomposites for Active Food Packaging Materials with Ethylene Scavenging and Gas Barrier Properties. *Food Bioprocess Technol.* **2017**, *10* (4), 789–798. https://doi.org/10.1007/s11947-017-1860-0.

(137) Tas, C. E.; Sevinis Ozbulut, E. B.; Ceven, O. F.; Tas, B. A.; Unal, S.; Unal, H. Purification and Sorting of Halloysite Nanotubes into Homogeneous, Agglomeration-Free Fractions by Polydopamine Functionalization. *ACS Omega* **2020**, *5* (29), 17962–17972. https://doi.org/10.1021/acsomega.0c01057.

(138) Alkan-Tas, B.; Durmus-Sayar, A.; Duman, Z. E.; Sevinis-Ozbulut, E. B.; Unlu, A.; Binay, B.; Unal, S.; Unal, H. Antibacterial Hybrid Coatings from Halloysite-

Immobilized Lysostaphin and Waterborne Polyurethanes. *Prog. Org. Coatings* **2021**, *156*, 106248. https://doi.org/10.1016/J.PORGCOAT.2021.106248.

(139) Alfieri, M. L.; Massaro, M.; d'Ischia, M.; D'Errico, G.; Gallucci, N.; Gruttadauria, M.; Licciardi, M.; Liotta, L. F.; Nicotra, G.; Sfuncia, G.; Riela, S. Site-Specific Halloysite Functionalization by Polydopamine: A New Synthetic Route for Potential near Infrared-Activated Delivery System. *J. Colloid Interface Sci.* **2022**, *606*, 1779–1791. https://doi.org/10.1016/J.JCIS.2021.08.155.

(140) Massaro, M.; Armetta, F.; Cavallaro, G.; Chillura Martino, D. F.; Gruttadauria, M.; Lazzara, G.; Riela, S.; d'Ischia, M. Effect of Halloysite Nanotubes Filler on Polydopamine Properties. *J. Colloid Interface Sci.* **2019**, *555*, 394–402. https://doi.org/10.1016/J.JCIS.2019.07.100.

(141) Hebbar, R. S.; Isloor, A. M.; Ananda, K.; Ismail, A. F. Fabrication of Polydopamine Functionalized Halloysite Nanotube/Polyetherimide Membranes for Heavy Metal Removal. *J. Mater. Chem. A* **2016**, *4* (3), 764–774. https://doi.org/10.1039/C5TA09281G.

(142) Zou, Y.; Chen, X.; Yang, P.; Liang, G.; Yang, Y.; Gu, Z.; Li, Y. Regulating the Absorption Spectrum of Polydopamine. *Sci. Adv.* **2020**, *6* (36), eabb4696. https://doi.org/10.1126/sciadv.abb4696.

(143) Wei, W.; Zhang, X.; Zhang, S.; Wei, G.; Su, Z. Biomedical and Bioactive Engineered Nanomaterials for Targeted Tumor Photothermal Therapy: A Review. **2019**. https://doi.org/10.1016/j.msec.2019.109891.

(144) Kampf, G.; Voss, A.; Scheithauer, S. Inactivation of Coronaviruses by Heat. *J. Hosp. Infect.* **2020**, *105*, 348–349. https://doi.org/10.1016/j.jhin.2020.03.025.

(145) Spengler, J. Indoor Air Pollution : A Public Health Perspective Author (s): John D . Spengler and Ken Sexton Published by : American Association for the Advancement of Science Stable URL : Http://Www.Jstor.Org/Stable/1691425. *Adv. Sci.* **2010**, *221* (4605), 9–17.

(146) Douglas W.Dockery, Sc.D; C.Arden Pope III, Ph.D; Xiping Xu, M.D, Ph.D, John D. Spenngler, Ph.D; James H.Ware, Ph.D; Martha E. Fay, M.P.H;Benjamin G. Ferris, Jr, M.D and Frank E. Speizer, M. . The New England Journal of

Medicine Downloaded from Nejm.Org at Arizona Health Sciences Center and UMC on August 13, 2013. For Personal Use Only. No Other Uses without Permission. Copyright © 1993 Massachusetts Medical Society. All Rights Reserved. *Massachusetts Med. Soc.* **1993**, *329* (24).

(147) Brunekreef, B.; Holgate, S. T. Air Pollution and Health. *Lancet* **2002**, *360* (9341), 1233–1242. https://doi.org/10.1016/S0140-6736(02)11274-8.

(148) Wargocki, P. The Effects of Ventilation in Homes on Health. *Int. J. Vent.* **2013**, *12* (2), 101–118. https://doi.org/10.1080/14733315.2013.11684005.

(149) Wargocki, P. Perceived Air Quality, Sick Building Syndrome (SBS) Symptoms and Productivity in an Office with Two Different Pollution Loads. *Indoor Air* **1999**, *9* (3), 165–179. https://doi.org/10.1111/j.1600-0668.1999.t01-1-00003.x.

(150) Godish, T. *Indoor Environmental Quality*; CRC Press, 2016. https://doi.org/10.1201/9781420056747.

(151) Jung, J. H.; Hwang, G. B.; Lee, J. E.; Bae, G. N. Preparation of Airborne Ag/CNT Hybrid Nanoparticles Using an Aerosol Process and Their Application to Antimicrobial Air Filtration. *Langmuir* **2011**, *27* (16), 10256–10264. https://doi.org/10.1021/la201851r.

(152) Hu, J.; Zhong, Z.; Zhang, F.; Xing, W.; Low, Z. X.; Fan, Y. Coating of ZnO Nanoparticles onto the Inner Pore Channel Surface of SiC Foam to Fabricate a Novel Antibacterial Air Filter Material. *Ceram. Int.* **2015**, *41* (5), 7080–7090. https://doi.org/10.1016/j.ceramint.2015.02.016.

(153) Hwang, G. B.; Lee, J. E.; Nho, C. W.; Lee, B. U.; Lee, S. J.; Jung, J. H.; Bae, G. N. Short-Term Effect of Humid Airflow on Antimicrobial Air Filters Using Sophora Flavescens Nanoparticles. *Sci. Total Environ.* **2012**, *421–422*, 273–279. https://doi.org/10.1016/j.scitotenv.2012.01.060.

(154) Zhang, Y.; Yuan, S.; Feng, X.; Li, H.; Zhou, J.; Wang, B. Preparation of Nanofibrous Metal-Organic Framework Filters for Efficient Air Pollution Control. *J. Am. Chem. Soc.* **2016**, *138* (18), 5785–5788. https://doi.org/10.1021/jacs.6b02553.

(155) Kelly, F. J.; Fussell, J. C. Improving Indoor Air Quality, Health and Performance within Environments Where People Live, Travel, Learn and Work. *Atmos. Environ.* **2019**, *200* (December 2018), 90–109. https://doi.org/10.1016/j.atmosenv.2018.11.058.

(156) Lowther, S. D.; Deng, W.; Fang, Z.; Booker, D.; Whyatt, D. J.; Wild, O.; Wang, X.; Jones, K. C. How Efficiently Can HEPA Purifiers Remove Priority Fine and Ultrafine Particles from Indoor Air? *Environ. Int.* **2020**, *144* (July). https://doi.org/10.1016/j.envint.2020.106001.

(157) Chuaybamroong, P.; Chotigawin, R.; Supothina, S.; Sribenjalux, P.; Larpkiattaworn, S.; Wu, C. Y. Efficacy of Photocatalytic HEPA Filter on Microorganism Removal. *Indoor Air* **2010**, *20* (3), 246–254. https://doi.org/10.1111/j.1600-0668.2010.00651.x.

(158) Mamaghani, A. H.; Haghighat, F.; Lee, C. S. Photocatalytic Oxidation Technology for Indoor Environment Air Purification: The State-of-the-Art. *Appl. Catal. B Environ.* **2017**, *203*, 247–269. https://doi.org/10.1016/j.apcatb.2016.10.037.

(159) Guieysse, B.; Hort, C.; Platel, V.; Munoz, R.; Ondarts, M.; Revah, S. Biological Treatment of Indoor Air for VOC Removal: Potential and Challenges. *Biotechnol. Adv.* **2008**, *26* (5), 398–410. https://doi.org/10.1016/j.biotechadv.2008.03.005.

(160) Kwong, C. W.; Chao, C. Y. H.; Hui, K. S.; Wan, M. P. Removal of VOCs from Indoor Environment by Ozonation over Different Porous Materials. *Atmos. Environ.* **2008**, *42* (10), 2300–2311. https://doi.org/10.1016/j.atmosenv.2007.12.030.

(161) Kujundzic, E.; Matalkah, F.; Howard, C. J.; Hernandez, M.; Miller, S. L. UV Air Cleaners and Upper-Room Air Ultraviolet Germicidal Irradiation for Controlling Airborne Bacteria and Fungal Spores. *J. Occup. Environ. Hyg.* **2006**, *3* (10), 536–546. https://doi.org/10.1080/15459620600909799.

(162) Li, P.; Li, J.; Feng, X.; Li, J.; Hao, Y.; Zhang, J.; Wang, H.; Yin, A.; Zhou, J.; Ma, X.; Wang, B. Metal-Organic Frameworks with Photocatalytic Bactericidal

Activity for Integrated Air Cleaning. *Nat. Commun.* **2019**, *10* (1), 1–10. https://doi.org/10.1038/s41467-019-10218-9.

(163) Li, J.; Dong, X.; Sun, Y.; Jiang, G.; Chu, Y.; Lee, S. C.; Dong, F. Tailoring the Rate-Determining Step in Photocatalysis via Localized Excess Electrons for Efficient and Safe Air Cleaning. *Appl. Catal. B Environ.* **2018**, *239*, 187–195. https://doi.org/10.1016/j.apcatb.2018.08.019.

(164) Wen, T. Y.; Wang, H. C.; Krichtafovitch, I.; Mamishev, A. V. Novel Electrodes of an Electrostatic Precipitator for Air Filtration. *J. Electrostat.* **2015**, *73*, 117–124. https://doi.org/10.1016/j.elstat.2014.11.002.

(165) Luengas, A.; Barona, A.; Hort, C.; Gallastegui, G.; Platel, V.; Elias, A. A Review of Indoor Air Treatment Technologies. *Rev. Environ. Sci. Biotechnol.* **2015**, *14* (3), 499–522. https://doi.org/10.1007/s11157-015-9363-9.

(166) Chong, E. seok; Hwang, G. B.; Nho, C. W.; Kwon, B. M.; Lee, J. E.; Seo, S. C.; Bae, G. N.; Jung, J. H. Antimicrobial Durability of Air Filters Coated with Airborne Sophora Flavescens Nanoparticles. *Sci. Total Environ.* **2013**, *444*, 110–114. https://doi.org/10.1016/j.scitotenv.2012.11.075.

(167) McFeters, G. A.; Stuart, D. G. Survival of Coliform Bacteria in Natural Waters: Field and Laboratory Studies with Membrane-Filter Chambers. *Appl. Microbiol.* **1972**, *24* (5), 805–811. https://doi.org/10.1128/am.24.5.805-811.1972.

(168) Ferdous, Z.; Nemmar, A. *Health Impact of Silver Nanoparticles: A Review of the Biodistribution and Toxicity Following Various Routes of Exposure*; 2020; Vol. 21. https://doi.org/10.3390/ijms21072375.

(169) Usachev, E. V.; Pyankov, O. V.; Usacheva, O. V.; Agranovski, I. E. Antiviral Activity of Tea Tree and Eucalyptus Oil Aerosol and Vapour. *J. Aerosol Sci.* **2013**, *59*, 22–30. https://doi.org/10.1016/j.jaerosci.2013.01.004.

(170) Pyankov, O. V.; Usachev, E. V.; Pyankova, O.; Agranovski, I. E. Inactivation of Airborne Influenza Virus by Tea Tree and Eucalyptus Oils. *Aerosol Sci. Technol.* **2012**, *46* (12), 1295–1302. https://doi.org/10.1080/02786826.2012.708948.

(171) Sim, K. M.; Kim, K. H.; Hwang, G. B.; Seo, S. C.; Bae, G. N.; Jung, J. H.

Development and Evaluation of Antimicrobial Activated Carbon Fiber Filters Using Sophora Flavescens Nanoparticles. *Sci. Total Environ.* **2014**, *493*, 291–297. https://doi.org/10.1016/j.scitotenv.2014.06.002.

(172) Choi, J.; Yang, B. J.; Bae, G. N.; Jung, J. H. Herbal Extract Incorporated Nanofiber Fabricated by an Electrospinning Technique and Its Application to Antimicrobial Air Filtration. *ACS Appl. Mater. Interfaces* **2015**, *7* (45), 25313–25320. https://doi.org/10.1021/acsami.5b07441.

(173) Sim, K. M.; Park, H. S.; Bae, G. N.; Jung, J. H. Antimicrobial Nanoparticle-Coated Electrostatic Air Filter with High Filtration Efficiency and Low Pressure Drop. *Sci. Total Environ.* **2015**, *533*, 266–274. https://doi.org/10.1016/j.scitotenv.2015.07.003.

(174) Komaladewi, A. A. I. A. S.; Khoiruddin, K.; Surata, I. W.; Subagia, I. D. G. A.; Wenten, I. G. Recent Advances in Antimicrobial Air Filter. *E3S Web of Conferences*. 2018. https://doi.org/10.1051/e3sconf/20186703016.

(175) Yuce, S.; Demirel, O.; Alkan Tas, B.; Sungur, P.; Unal, H. Halloysite Nanotube/Polydopamine Nanohybrids as Clay-Based Photothermal Agents for Antibacterial Applications. *ACS Appl. Nano Mater.* **2021**, *4* (12), 13432–13439. https://doi.org/10.1021/acsanm.1c02936.